NATIONAL ADVISORY COMMITTEE FOR AERONAUTICS

TECHNICAL NOTE 2346

AN ITERATIVE TRANSFORMATION PROCEDURE FOR NUMERICAL SOLUTION OF FLUTTER AND SIMILAR CHARACTERISTIC-VALUE PROBLEMS

By Myron L. Gossard

Langley Aeronautical Laboratory
Langley Field, Va.

Washington
May 1951

NATIONAL ADVISORY COMMITTEE FOR AERONAUTICS

TECHNICAL NOTE 2346

AN ITERATIVE TRANSFORMATION PROCEDURE FOR NUMERICAL SOLUTION OF FLUTTER AND SIMILAR CHARACTERISTIC-VALUE PROBLEMS

By Myron L. Gossard

SUMMARY

An iterative transformation procedure suggested by H. Wielandt for numerical solution of flutter and similar characteristic-value problems is presented. Application of this procedure to ordinary natural-vibration problems and to flutter problems is shown by numerical examples. Comparisons of computed results with experimental values and with results obtained by other methods of analysis are made.

INTRODUCTION

Existing methods of flutter analysis include the representative-section method, generalized-coordinate methods, matrix methods, and operational methods. The present paper presents an iteration procedure for analysis of flutter and similar characteristic-value problems.

For ordinary natural-vibration problems, iterative procedures of the Stodola type (references 1 and 2) are suitable for finding the fundamental and higher-order natural modes and frequencies. The higher-order solutions are obtained through use of the orthogonality relations that exist among the natural modes.

Orthogonality relations analogous to those that exist in ordinary vibration problems can be found in the flutter problem only by introduction of the so-called "adjoint" problem. (This additional step is unnecessary in ordinary vibration problems by virtue of the fact that they are "self-adjoint.") Wielandt has suggested an iterative transformation procedure (reference 3) which is well-suited to the flutter problem in that it avoids the need of orthogonality relations and hence does not require consideration of the adjoint problem. The iterative transformation procedure can also be applied to ordinary natural-vibration problems with less labor than is generally required in the extended Stodola procedure.

Because both the original and translated works of Wielandt are difficult to follow, an explanation of the idea of the iterative transformation procedure is given in the present paper and the application of the procedure to ordinary natural-vibration problems and to flexure-torsion flutter problems is shown in numerical examples. Comparisons of computed results with experimental values and with results obtained by other methods of analysis are also made.

SYMBOLS

EI	flexural stiffness
GJ	torsional stiffness
x	spanwise coordinate with origin at root of wing
y	complex representation of amplitudes and phases of translation of elastic axis in harmonic motion
ϕ	complex representation of amplitudes and phases of rotation about elastic axis in harmonic motion
w	coupled mode (y,ϕ)
P_y	complex coefficients of y which, when multiplied by y, give complex representation of amplitudes and phases of aerodynamic and inertia forces associated with translational component of harmonic motion
P_ϕ	complex coefficients of ϕ which, when multiplied by ϕ, give complex representation of amplitudes and phases of aerodynamic and inertia forces associated with rotational component of harmonic motion
Q_y	complex coefficients of y which, when multiplied by y, give complex representation of amplitudes and phases of aerodynamic and inertia torques associated with translational component of harmonic motion
Q_ϕ	complex coefficients of ϕ which, when multiplied by ϕ, give complex representation of amplitudes and phases of aerodynamic and inertia torques associated with rotational component of harmonic motion
g_y, g_ϕ	structural-damping coefficients associated with flexure and torsion, respectively (see appendix B)

g_a coefficient of artificial damping (may be either positive or negative)

k reduced frequency $(b\omega/v)$

ω frequency of harmonic motion

C characteristic value $\left(\frac{1 + ig_a}{\omega^2}\right)$

b length of semichord of wing

L length of cantilever wing from root to tip

μ mass ratio $(\gamma/\pi\rho b^2)$

v velocity of air relative to wing

γ distributed mass of wing per unit length of span

ρ mass density of air

a distance between midchord axis and elastic axis in terms of local semichord, positive when elastic axis is behind midchord axis

u distance between elastic axis and gravity axis of distributed mass of wing in terms of local semichord, positive when gravity axis is behind elastic axis

r radius of gyration of distributed mass of wing about elastic axis in terms of local semichord

F,G transcendental functions of k (see reference 4)

t time

F_{mn} eigenvalue factor $\left(\frac{C_m}{C_n} - 1\right)$

R ratio of complex constants

λ length; in numerical solutions, distance between specific adjacent stations of wing

p applied force

q	applied torque
V	shear
M	bending moment
α	curvature
β	slope of elastic axis
T	twisting moment
θ	angle of twist

Subscripts:

1,2,3,...	true modes or eigenvalues
a2,a3,a4,...	transformed modes
b	intermediate derived mode
A,B,C,...	stations
R	real
I	imaginary
o	reference value
b1,ba2,ba3,...	sweeping functions

Superscripts:

(1),(2),(3),...	cycles of iteration

A bar over a symbol indicates a concentrated quantity instead of a distributed quantity.

A prime is used to denote division by ω^2.

ITERATIVE TRANSFORMATION METHOD OF SOLUTION

General Features of Method

The principle of the iterative transformation procedure is similar in form to that of the standard iteration procedure for solving characteristic-value problems. Both procedures require the determination of the solutions in the order of the magnitudes of the eigenvalues, beginning with the fundamental. Both procedures require assumptions of modes, integrations which generally must be done numerically, and sweeping operations for higher-order-mode determinations. The distinguishing features of the iterative transformation procedure occur in the determination of solutions higher than the fundamental and are as follows: (1) The immediate aim is to determine not the true nth mode, as in the standard iteration procedure, but a particular linear combination composed of all modes from the fundamental to the nth. This linear combination is referred to as the transformed nth mode. The transformed nth mode can be made to have nodal (zero) points at specified stations of the wing; such a feature is highly desirable in numerical work. (2) The sweeping operations, which consist of subtractions of lower-order-mode shapes from the function obtained by integrating the assumed mode, do not employ the orthogonality relations as in the standard iteration method but make use of forcing functions that, in numerical work, greatly simplify the sweeping operations and increase the overall accuracy of the results by making the sweeping operations more consistent with the rest of the process. (3) Although the true nth eigenvalue is determined directly in the iterative transformation procedure, the true nth mode must be computed from quantities within the iteration cycle after the transformed nth mode is found.

Outline of Steps in the Procedure

The equation of equilibrium of a cantilever beam vibrating harmonically in pure flexure is

$$\frac{d^2}{dx^2} EI \frac{d^2y}{dx^2} = \gamma\omega^2 y \tag{1}$$

or, after integration with proper attention to boundary conditions,

$$y = \int_0^x \int_0^x \frac{1}{EI} \int_x^L \int_x^L \gamma\omega^2 y (dx)^4 \tag{2}$$

The solutions of this integral equation are the true natural modes (eigenfunctions) y_1, y_2, y_3, . . . and the corresponding natural frequencies (eigenvalues) ω_1, ω_2, ω_3, ... For convenience in subsequent discussion, the true modes are assumed to be normalized to unity at some position (station A) along the beam.

The first mode and frequency are assumed to have been previously determined by the Stodola process. The iterative transformation procedure becomes applicable in the determination of the second mode and frequency. As mentioned previously, the immediate aim in the iteration for the second mode is the determination of a linear combination of first and second modes which is called the transformed second mode. The linear combination $y_2 - y_1$ which has zero ordinate at station A is chosen and defined as the transformed second mode to be determined. The iteration for determination of this transformed second mode may be described as follows:

(1) A plausible shape $y_{a2}^{(1)}$ for the transformed second mode is assumed. This shape must have zero ordinate at station A and should satisfy the boundary conditions as closely as possible.

(2) The displacement

$$y_b = \int_0^x \int_0^x \frac{1}{EI} \int_x^L \int_x^L \gamma \omega_2^2 y_{a2}^{(1)} (dx)^4$$

resulting from the inertia load $\gamma \omega_2^2 y_{a2}^{(1)}$ corresponding to the assumed shape $y_{a2}^{(1)}$ vibrating harmonically at frequency ω_2 is calculated. This calculation must usually be done numerically with the square of the frequency $\left(\omega_2^2\right)$ being carried along as an undetermined factor.

(3) A first-mode shape (previously determined) is subtracted (swept out) from the calculated displacement y_b in an amount such that the resulting displacement is zero at station A. Thus the resulting displacement is

$$y_{a2}^{(2)} = y_b - \left(\frac{y_b}{y_1}\right)_A y_1$$

(4) The resulting displacement $y_{a2}^{(2)}$ is compared with the assumed displacement $y_{a2}^{(1)}$. When the computations are numerical, the

ratios $y_{a2}^{(2)}/y_{a2}^{(1)}$ are compared at all the stations. If the assumed displacement is exactly equal to the transformed second mode, the ratios are equal to each other. These ratios contain the single unknown ω_2, and the second frequency is that value of ω_2 which makes the ratios unity.

(5) If the ratios $y_{a2}^{(2)}/y_{a2}^{(1)}$ from the first cycle of iteration outlined in the four preceding steps are not reasonably the same at all stations, the process must be repeated until the ratios become reasonably the same. Each new cycle starts with the resultant displacement of each preceding cycle. The convergence of this process to the second frequency and the transformed second mode is proved in appendix A.

The transformed third mode and the third frequency are computed in the following manner. The transformed third mode is defined as that combination of the first three natural modes which has a zero ordinate at the same station that was used in the transformed second mode (station A) and also a zero ordinate at some other station, station B. Thus the transformed third mode is defined as

$$y_3 - y_1 - \left(\frac{y_3 - y_1}{y_2 - y_1}\right)_B \left(y_2 - y_1\right)$$

The iteration is as follows:

(1) A plausible shape $y_{a3}^{(1)}$ for the transformed third mode is assumed. This shape must have zero ordinates at stations A and B and should satisfy the boundary conditions as closely as possible.

(2) The displacement

$$y_b = \int_0^x \int_0^x \frac{1}{EI} \int_x^L \int_x^L \gamma \omega_3^2 y_{a3}^{(1)} (dx)^4$$

is calculated, with the square of the frequency $\left(\omega_3^2\right)$ carried along as an undetermined factor.

(3) The first of two sweeping operations, in which a first-mode shape is swept from the displacement y_b so as to make the resulting

displacement at station A zero, is performed. This operation gives the displacement

$$y_b - \left(\frac{y_b}{y_1}\right)_A y_1$$

(4) The second sweeping operation, in which a transformed-second-mode shape (previously determined) is swept from the resulting displacement of step (3) so that the new resulting displacement is zero at station B as well as at station A, is performed. (This second sweeping operation cannot disturb the zero condition at station A established in step (3) because the second sweeping function (the transformed second mode) is identically zero at station A.) Thus, the final resulting displacement is

$$y_{a3}^{(2)} = y_b - \left(\frac{y_b}{y_1}\right)_A y_1 - \left[\frac{y_b - \left(\frac{y_b}{y_1}\right)_A y_1}{y_{a2}}\right]_B y_{a2}$$

(5) Comparisons of the ratios $y_{a3}^{(2)}/y_{a3}^{(1)}$ at all stations are made, and, if they are not reasonably the same, additional cycles of iteration are carried out until the ratios become reasonably the same. The third frequency is then computed from the ratios as explained previously. Convergence of this process to the third frequency and the transformed third mode is proved in appendix A.

Frequencies and transformed modes higher than the third may be computed by extensions of the process just described.

Physical Interpretation of the Procedure

A physical interpretation of the iterative transformation procedure can be given. With regard to the transformed second mode, for example, the following question may be asked: Under what conditions can the beam vibrate in the transformed-second-mode shape at the second natural frequency? Vibration in shape $y_{a2} = y_2 - y_1$ at frequency ω_2 implies an inertia loading $\gamma\omega_2^2(y_2 - y_1)$. But if this load is substituted in place of $\gamma\omega_2^2 y$ in the right-hand side of equation (2), the result after integration will not be $y_2 - y_1$ but

$$y_2 - \frac{\omega_2^2}{\omega_1^2} y_1 = \int_0^x \int_0^x \frac{1}{EI} \int_x^L \int_x^L \gamma \omega_2^2 \left(y_2 - y_1\right) (dx)^4 \qquad (3)$$

However, if an external (forcing) load of an amount $\gamma\left(\omega_2^2 - \omega_1^2\right)y_1$ is added to the inertia load, the total load $\gamma\left(\omega_2^2 y_2 - \omega_1^2 y_1\right)$ will produce the shape $y_2 - y_1$. Thus

$$\int_0^x \int_0^x \frac{1}{EI} \int_x^L \int_x^L \gamma \left(\omega_2^2 y_2 - \omega_1^2 y_1\right) (dx)^4 = y_2 - y_1 \qquad (4)$$

The inertia and forcing loads are illustrated in figure 1. The inertia load acting alone produces a displacement (equation (3)) generally different from zero at station A. The forcing load produces the displacement

$$\left(\frac{\omega_2^2}{\omega_1^2} - 1\right) y_1 = \int_0^x \int_0^x \frac{1}{EI} \int_x^L \int_x^L \gamma \left(\omega_2^2 - \omega_1^2\right) y_1 (dx)^4 \qquad (5)$$

This displacement (equal to the sweeping function) has the shape of the previously determined first mode and is equal and opposite at station A to the displacement due to the inertia load; that is, by virtue of the previously assigned normalizations at station A,

$$\left(\frac{\omega_2^2}{\omega_1^2} - 1\right)\left(y_1\right)_A = -\left(y_2 - \frac{\omega_2^2}{\omega_1^2} y_1\right)_A \qquad (6)$$

Thus the displacement due to the forcing load is completely determined when the displacement due to the inertia load is known. The gist of the foregoing analysis is that vibration in the transformed-second-mode shape is the response of the beam to an oscillatory forcing load of the first-mode shape and of frequency equal to the second natural frequency, superimposed on a free vibration of the beam in the second natural mode.

Similar physical interpretations of the iterative transformation process for modes higher than the second can be made.

Application of the Procedure in Ordinary Coupled Natural-Vibration Problems

The procedure that has been outlined in a preceding section for pure flexure can easily be extended to systems capable of simultaneous

flexural and torsional displacements. Airplane wings belong to the latter class of systems. The only distinguishing element in coupled flexural-torsional vibration problems is that each natural mode contains two components, the flexure and the torsion. These components must always appear together in a fixed relation to each other. The two components must be computed together and must be used together.

Each coupled mode is a solution of the simultaneous differential equations

$$\frac{d^2}{dx^2} EI \frac{d^2y}{dx^2} = \gamma\omega^2(y + bu\phi) \tag{7}$$

$$- \frac{d}{dx} GJ \frac{d\phi}{dx} = \gamma\omega^2\left(buy + b^2r^2\phi\right) \tag{8}$$

Equations (7) and (8), after integration, become (for a cantilever beam)

$$y = \int_0^x \int_0^x \frac{1}{EI} \int_x^L \int_x^L \gamma\omega^2(y + bu\phi)(dx)^4 \tag{9}$$

$$\phi = \int_0^x \frac{1}{GJ} \int_x^L \gamma\omega^2(buy + b^2r^2\phi)(dx)^2 \tag{10}$$

The solution of the integral equations (9) and (10) for the coupled transformed second mode by the iterative transformation procedure is outlined diagrammatically in figure 2. The flexural component of the displacement for a particular step is illustrated in the left-hand side of the figure and the torsional component is illustrated at the same level in the right-hand side.

In the first step, an approximation to a linear combination of the true first and second coupled modes is assumed. The particular linear combination having zero flexural displacement at the tip station (station A) is chosen. (For greatest numerical accuracy, this nodal point should be chosen in the component and at the station where the first coupled mode has its maximum numerical value.) The symbols $y_{a2}^{(1)}$ and $\phi_{a2}^{(1)}$ are used to designate the flexural and torsional components of this assumed displacement, respectively. In general, the magnitude of the torsional component relative to the flexural component is

difficult to estimate; the most expedient thing to do is take one of the components equal to zero.

The second step is the computation (by numerical integration) of the two components of the displacement due to the inertia forces $\gamma\omega_2^2\left(y_{a2} + bu\phi_{a2}\right)$ and inertia torques $\gamma\omega_2^2\left(buy_{a2} + b^2r^2\phi_{a2}\right)$ that are associated with the assumed displacement. The result is termed the intermediate derived mode, and the symbols $y_b^{(1)}$ and $\phi_b^{(1)}$ are used to designate its two components.

The third step is the determination of a sweeping function having the shape of the first coupled mode (previously determined) and a magnitude such that the sum of the intermediate derived mode and the sweeping function equals zero in the flexural component at station A. In algebraic terms, the first-mode sweeping function is given by

$$y_{b1}^{(1)} = -\left(\frac{y_b^{(1)}}{y_1}\right)_A y_1 \tag{11}$$

$$\phi_{b1}^{(1)} = -\left(\frac{y_b^{(1)}}{y_1}\right)_A \phi_1 \tag{12}$$

The fourth step is the addition of the intermediate derived mode and the first-mode sweeping function to give the derived transformed second mode. Thus the two components of the derived transformed second mode are

$$y_{a2}^{(2)} = y_b^{(1)} - \left(\frac{y_b^{(1)}}{y_1}\right)_A y_1 \tag{13}$$

$$\phi_{a2}^{(2)} = \phi_b^{(1)} - \left(\frac{y_b^{(1)}}{y_1}\right)_A \phi_1 \tag{14}$$

The calculation of the ratios $y_{a2}^{(2)}/y_{a1}^{(1)}$ and $\phi_{a2}^{(2)}/\phi_{a2}^{(1)}$ at all stations completes the first cycle of iteration.

Additional cycles are carried out until the ratios at all stations in both the flexural and torsional components have values that are reasonably the same. The true second natural frequency of the coupled system is then obtained as described previously.

Steady vibration of an airplane wing at zero airspeed is an example of coupled natural vibration. The actual numerical calculations for the transformed second mode as well as for the first mode and transformed third mode of an airplane wing vibrating at zero airspeed are discussed subsequently as a special case of flutter.

The more general equations of airplane flutter at nonzero airspeed may be interpreted in such a way that they can be solved by a process analogous to that just described for coupled natural vibration.

APPLICATION OF THE ITERATIVE TRANSFORMATION METHOD TO FLUTTER

Flutter Equations

The differential equations of equilibrium for a wing executing simple harmonic motion are

$$\frac{d^2}{dx^2} EI\left(1 + ig_y\right)\frac{d^2y}{dx^2} = P_y y + P_\phi \phi \tag{15}$$

$$-\frac{d}{dx} GJ\left(1 + ig_\phi\right)\frac{d\phi}{dx} = Q_y y + Q_\phi \phi \tag{16}$$

These equations govern a motion represented by

$$Y(x,t) = y(x)e^{i\omega t} \tag{17}$$

$$\Phi(x,t) = \phi(x)e^{i\omega t} \tag{18}$$

The use of the structural-damping coefficients g_y and g_ϕ in equations (15) and (16) is discussed in appendix B. The expressions $P_y y + P_\phi \phi$ and $Q_y y + Q_\phi \phi$ are the intensities of applied force and torque, respectively. For aerodynamic and inertia forces and torques

due to air flow and distributed mass, the P and Q coefficients have values given by the following formulas (rearranged from those in reference 4): For P_y,

$$P_y \equiv P_{Ry} - iP_{Iy} \tag{19}$$

in which

$$P_{Ry} = \left(\frac{b}{b_o}\right)^2\left(\frac{2G}{k} + 1 + \mu\right)\left(\frac{\gamma}{\mu}\right)_o\omega^2 \tag{20}$$

and

$$P_{Iy} = \left(\frac{b}{b_o}\right)^2 \frac{2F}{k}\left(\frac{\gamma}{\mu}\right)_o\omega^2 \tag{21}$$

For P_ϕ,

$$P_\phi \equiv P_{R\phi} - iP_{I\phi} \tag{22}$$

in which

$$P_{R\phi} = \left(\frac{b}{b_o}\right)^3\left[\left(\frac{1}{2} - a\right)\frac{2G}{k} - \frac{2F}{k^2} - a + \mu u\right]\left(\frac{\gamma}{\mu}\right)_o b_o\omega^2 \tag{23}$$

and

$$P_{I\phi} = \left(\frac{b}{b_o}\right)^3\left[\frac{1}{k} + \frac{2G}{k^2} + \left(\frac{1}{2} - a\right)\frac{2F}{k}\right]\left(\frac{\gamma}{\mu}\right)_o b_o\omega^2 \tag{24}$$

For Q_y,

$$Q_y \equiv Q_{Ry} - iQ_{Iy} \tag{25}$$

in which

$$Q_{Ry} = \left(\frac{b}{b_o}\right)^3\left[-\left(\frac{1}{2} + a\right)\frac{2G}{k} - a + \mu u\right]\left(\frac{\gamma}{\mu}\right)_o b_o\omega^2 \tag{26}$$

and

$$Q_{Iy} = \left(\frac{b}{b_o}\right)^3\left[-\left(\frac{1}{2} + a\right)\frac{2F}{k}\right]\left(\frac{\gamma}{\mu}\right)_o b_o\omega^2 \tag{27}$$

And for Q_ϕ,

$$Q_\phi \equiv Q_{R\phi} - iQ_{I\phi} \tag{28}$$

in which

$$Q_{R\phi} = \left(\frac{b}{b_o}\right)^4\left[-\left(\frac{1}{4} - a^2\right)\frac{2G}{k} + \left(\frac{1}{2} + a\right)\frac{2F}{k^2} + \frac{1}{8} + a^2 + \mu r^2\right]\left(\frac{\gamma}{\mu}\right)_o b_o{}^2\omega^2 \tag{29}$$

and

$$Q_{I\phi} = \left(\frac{b}{b_o}\right)^4\left[\left(\frac{1}{2} - a\right)\frac{1}{k} - \left(\frac{1}{2} + a\right)\frac{2G}{k^2} - \left(\frac{1}{4} - a^2\right)\frac{2F}{k}\right]\left(\frac{\gamma}{\mu}\right)_o b_o{}^2\omega^2 \tag{30}$$

For inertia forces and torques due to concentrated mass, the intensities of force and torque are, respectively,

$$P_y y + P_\phi \phi = \lim_{dx\to 0} \frac{\overline{P_y} y + \overline{P_\phi}\phi}{dx} \tag{31}$$

and

$$Q_y y + Q_\phi \phi = \lim_{dx\to 0} \frac{\overline{Q_y} y + \overline{Q_\phi}\phi}{dx} \tag{32}$$

in which

$$\overline{P_y} = \left(\frac{b}{b_o}\right)^2\left(\mu\,\frac{\overline{\gamma}}{\gamma\lambda_o}\right)\lambda_o\left(\frac{\gamma}{\mu}\right)_o\omega^2 \tag{33}$$

$$\overline{P_\phi} = \overline{Q_y} = \left(\frac{b}{b_o}\right)^3\left(\mu\,\frac{\overline{\gamma}}{\gamma\lambda_o}\,\overline{u}\right)\lambda_o\left(\frac{\gamma}{\mu}\right)_o b_o\omega^2 \tag{34}$$

and

$$Q_\phi = \left(\frac{b}{b_o}\right)^4\left(\mu\,\frac{\overline{\gamma}}{\gamma\lambda_o}\,\overline{r}^2\right)\lambda_o\left(\frac{\gamma}{\mu}\right)_o b_o{}^2\omega^2 \tag{35}$$

For a cantilever wing the boundary conditions on the displacements are

$$(y)_{x=0} = (\phi)_{x=0} = \left(\frac{dy}{dx}\right)_{x=0} = \left[EI\left(1 + ig_y\right)\frac{d^2y}{dx^2}\right]_{x=L} =$$

$$\left[\frac{d}{dx}EI\left(1 + ig_y\right)\frac{d^2y}{dx^2}\right]_{x=L} = \left[GJ\left(1 + ig_\phi\right)\frac{d\phi}{dx}\right]_{x=L} = 0 \qquad (36)$$

The differential equations (15) and (16) are now written with the eigenvalue ω^2 as an explicit factor. Thus equations (15) and (16) become

$$\frac{d^2}{dx^2}EI\left(1 + ig_y\right)\frac{d^2y}{dx^2} = \omega^2\left(P_y'y + P_\phi'\phi\right) \qquad (37)$$

and

$$-\frac{d}{dx}GJ\left(1 + ig_\phi\right)\frac{d\phi}{dx} = \omega^2\left(Q_y'y + Q_\phi'\phi\right) \qquad (38)$$

in which the P' and Q' coefficients are equal, respectively, to the P and Q coefficients divided by ω^2.

Formulation of Pseudoflutter Problem

Those solutions ω^2, (y,ϕ) of equations (37) and (38) for which ω^2 is a real and positive (not complex) quantity represent the steady harmonic motions of true flutter. However, because the P and Q coefficients are in general complex and because of the presence of structural damping, the solutions of equations (37) and (38) will, in general, be complex and will include complex eigenvalues ω^2. As in other methods of flutter analysis, the problem is made tractable by assuming at the beginning a value of the parameter $k = \frac{b\omega}{v}$. This assumption fixes the values of the P and Q coefficients. A real value of k is assumed because v must be real and only real values of ω can represent flutter. To avoid the inconsistence of assumed real values of k and obtained complex values of ω^2 in the solutions, the problem itself is altered by introducing an artificial damping so that the complex eigenvalue is given by $\frac{\omega^2}{1 + ig_a}$, where g_a is the coefficient of artificial damping. Thus the differential equations of what may be termed the pseudoflutter problem become

$$\frac{d^2}{dx^2} EI\left(1 + ig_y\right)\frac{d^2y}{dx^2} = \frac{\omega^2}{1 + ig_a}\left(P_y'y + P_\phi'\phi\right) \tag{39}$$

$$-\frac{d}{dx} GJ\left(1 + ig_\phi\right)\frac{d\phi}{dx} = \frac{\omega^2}{1 + ig_a}\left(Q_y'y + Q_\phi'\phi\right) \tag{40}$$

The value of ω^2 can now be real for any assumed real value of k and is therefore the square of the frequency of the steady harmonic motion maintained by the artificial-damping forces and the naturally present aerodynamic, inertia, structural, and structural-damping forces. True flutter is possible for those special cases in which g_a is zero.

Equations (39) and (40) are similar in form to equations (7) and (8) and can be solved by the iterative transformation procedure in a way completely analogous to the solution of the ordinary problem. The complications introduced by the presence of air forces require, however, that a set of solutions be obtained for each of several assumed values of k. The fact that most of the functions involved are complex virtually quadruples the labor as compared with that required in the ordinary coupled natural-vibration problem.

Steps in the Iteration as Applied to Flutter

The iteration procedure employs the basic differential equations (39) and (40) in their integral forms which, for the cantilever wing under consideration, are

$$y = \frac{1}{C}\int_0^x\int_0^x \frac{1}{EI\left(1 + ig_y\right)}\int_x^L\int_x^L \left(P_y'y + P_\phi'\phi\right)(dx)^4 \tag{41}$$

$$\phi = \frac{1}{C}\int_0^x \frac{1}{GJ\left(1 + ig_\phi\right)}\int_x^L \left(Q_y'y + Q_\phi'\phi\right)(dx)^2 \tag{42}$$

in which C stands for the more convenient form $\frac{1 + ig_a}{\omega^2}$ of the eigenvalue. The iteration of equations (41) and (42) follows the same form as the iteration of equations (9) and (10). Briefly, the steps are as follows:

(1) A real value of k is assumed and the values of the complex P and Q coefficients are computed.

(2) An assumption is made for the desired mode y,ϕ. (In the first cycle of iteration the assumed mode may be real but in the following cycles it will be complex.)

(3) The complex loadings $P_y y + P_\phi \phi$ and $Q_y y + Q_\phi \phi$ are computed.

(4) The integrations indicated in the equations are carried out numerically to get the complex intermediate derived mode.

(5) The sweeping operations are performed by using the complex lower-order transformed modes previously determined. For convenience in numerical calculations, the flexural and torsional components of the complex derived (swept) transformed mode are computed in the forms

$$\frac{1}{C}\frac{\gamma_o}{\mu_o}\frac{L^4}{E_o I_o} b_o K_y \tag{43}$$

and

$$\frac{1}{C}\frac{\gamma_o}{\mu_o}\frac{L^4}{E_o I_o}\frac{E_o I_o}{G_o J_o}\frac{b_o^2}{L^2} K_\phi \tag{44}$$

respectively, in which K_y and K_ϕ are nondimensional complex functions of the spanwise coordinate x.

(6) The derived and assumed modes are compared by computing their ratios at the stations of the wing. If these ratios are not reasonably the same, additional cycles of iteration are carried out until the ratios are reasonably the same. In the limit (never obtained in practice) the ratios will be identical and the proper value of C is that value which makes them unity; that is,

$$\frac{\frac{1}{C}\frac{\gamma_o}{\mu_o}\frac{L^4}{E_o I_o} b_o K_y}{y} = \frac{\frac{1}{C}\frac{\gamma_o}{\mu_o}\frac{L^4}{E_o I_o}\frac{E_o I_o}{G_o J_o}\frac{b_o^2}{L^2} K_\phi}{\phi} = 1 \tag{45}$$

in which y and ϕ constitute the assumed mode of the limiting cycle and the functions in the numerators constitute the derived mode of the limiting cycle.

Equation (45) may be stated in the form

$$\frac{1}{C}(D + iH)\frac{\gamma_o}{\mu_o}\frac{L^4}{E_oI_o} = 1 \tag{46}$$

in which D and H are nondimensional real numbers. Inasmuch as C is defined as $\frac{1 + ig_a}{\omega^2}$, equation (46) may be written

$$(D + iH)\frac{\gamma_o}{\mu_o}\frac{L^4}{E_oI_o} = \frac{1 + ig_a}{\omega^2} \tag{47}$$

from which the frequency and artificial-damping coefficient are obtained as follows:

$$\omega = \sqrt{\frac{\frac{E_oI_o}{L^4}\frac{\mu_o}{\gamma_o}}{D}} \tag{48}$$

$$g_a = \frac{H}{D} \tag{49}$$

The relative air velocity corresponding to the assumed value of k is given through the definition of k, that is,

$$v = \frac{b\omega}{k} \tag{50}$$

NUMERICAL EXAMPLES

Numerical computations presented in this section illustrate the actual application of the iterative transformation procedure first to the ordinary natural-vibration problem (vibration at zero airspeed) and then to the flutter problem. All examples deal with the cantilever wing shown in figure 3.

The geometric, structural, and mass properties of the wing are given in figure 3. A station coordinate system is employed for the purposes of the required numerical integrations. Four stations along the span have been selected as indicated in the figure; one of these stations is located at the spanwise position of the concentrated mass. The

distributions of forces and displacements over the span are considered to be adequately defined (through interpolation) by the forces and displacements at the four selected stations. The selection of a system of stations in any problem is important because it greatly influences the amount and accuracy of the work to follow. In problems, such as the present one, that involve concentrated masses, a station must be placed at each concentrated mass because displacements at the concentrated masses must be known. (More generally, a station must be placed at each discontinuity. Discontinuities may be present in the distribution of the structural stiffness and in the plan form as well as in distribution of mass.) The other stations should be equally spaced between the discontinuities, and for the system of parabolic interpolation used in the numerical integrations in this paper there must be a minimum of one station between each adjacent pair of discontinuities. The total number of stations should be the smallest possible that is consistent with the desired accuracy because the calculation effort increases rapidly with an increasing number of stations. In coupled systems, the number of degrees of freedom allowed is twice the number of stations selected; that is, the number of degrees of freedom in either the flexural or torsional component of displacement is equal to the number of stations employed. Experience has indicated that with parabolic approximations results accurate to at least two significant figures in the highest mode computed can be obtained by employing numbers of stations as follows: For uncoupled systems, the number of stations should be two greater than the order of the highest mode to be computed; for coupled systems, the number of stations should be one greater than the order of the highest mode to be computed, with a minimum of three stations. More than these minimum numbers of stations may be required if their use is dictated by sufficiently many discontinuities.

Ordinary Coupled Natural Modes and Frequencies

The calculations for the first, second, and third modes at zero airspeed for the wing of figure 3 are shown in tables 1, 2, and 3, respectively. In this case $k = \infty$ and the only aerodynamic forces are the apparent-mass forces. For simplicity, structural damping is disregarded; therefore, all quantities entering the problem are real. The numerical values of the aerodynamic-inertia force coefficients for $k = \infty$, as well as for other values of k to be used subsequently, are given in table 4.

The first coupled mode is computed in table 1. Table 1 shows in separate tabulations the flexural and torsional parts of the calculation. The first cycle of iteration (part (a) of the table) is shown in full detail. Two forms for the torsional part of the calculation are shown: The first form may be used when the torsional stiffness GJ is constant over each bay or over the whole length of the wing; the second form,

which requires slightly more work, must be used when GJ is variable and may be used, as in this case, when GJ is constant. The second and third cycles of iteration are summarized in parts (b) and (c) of table 1.

Details of the first cycle of iteration, if the procedure that applies only for constant torsional stiffness GJ for the torsional part of the calculation is used, are as follows: In columns 1 of table 1(a) the two parts $y_1^{(1)}$ and $\phi_1^{(1)}$ of the assumed first mode are listed. The torsional component is assumed to be zero because it will ultimately be small and is difficult to estimate. Columns 2 and 3 are the appropriate products of the assumed mode and the distributed-force coefficients. Columns 4, which are the sums of columns 2 and 3, give the two components of the external load which correspond to the assumed mode and the arbitrary frequency ω. Columns 5 give the concentrated loads (external forces and torques) that are equivalent to the distributed loads of columns 4. These equivalent concentrations are given in columns 5 in terms of the pertinent distances between stations λ_i and in columns 6 in terms of the reference distance λ_o. Formulas used for computing the equivalent concentrations from the distributed loads are given in appendix C. Columns 7 and 8 are the appropriate products of the assumed mode and the concentrated-force coefficients. Columns 9 are the total concentrated loads, the sums of columns 6, 7, and 8.

The flexural and torsional calculations must now be described separately. In column 10 for flexure, the average shears in the bays between stations are found by a successive summation of the concentrated loads from the tip where the shear is zero inboard to the root. In column 11 the increments of bending moment are computed by multiplying the shears by the bay lengths in terms of λ_o. The bending moments of column 12 are found by a successive summation of the increments of bending moment from the tip where the bending moment is zero inboard to the root. Column 13 gives the distribution of curvature, which is obtained by dividing each ordinate of the bending-moment curve by the local value of EI (EI in this example is constant). Equivalent concentrated curvatures are now obtained by applying to the distributed curvatures the previously used formulas for equivalent concentrations. Column 14 gives these equivalent concentrations in terms of the distances λ_i, and column 15 gives them in terms of the reference distance λ_o. The average slopes in the bays are obtained in column 16 by a successive summation of the concentrated curvatures from the root where the slope is zero outboard to the tip. The increments of derived flexural displacement are computed in column 17 by multiplying the average slopes by the bay lengths in terms of λ_o. The flexural component $y_1^{(2)}$ of the derived mode is obtained in column 18 by a successive summation of the increments of displacement from the root where the

displacement is zero outboard to the tip. Column 19 gives the ratios at the selected stations of the derived flexural component to the assumed flexural component.

Columns 10 to 15 for torsion are now considered. Column 10 gives the average twisting moments in the bays of the wing and is obtained by a successive summation of the concentrated torques of column 9 from the tip where the twisting moment is zero inboard to the root. The average twists in the bays are computed in column 11 by dividing the average twisting moment in each bay by the local value of GJ (GJ in this example is constant over the whole span). The increments of derived torsional displacement are obtained in column 12 by multiplying the average twists by the bay lengths in terms of λ_o. The torsional component of the derived mode is computed in column 13 by a successive summation of the increments of displacement from the root where the displacement is zero outboard to the tip. Inasmuch as the derived displacement of column 13 is in terms of GJ, the displacement is converted into terms of EI in column 14 so that it may be compared with the assumed torsional displacement on the same basis as the assumed and derived flexural displacements are compared and so that the next cycle may be started with displacement components having the same dimensions as the assumed mode of this first cycle. Column 15 normally would contain the ratios at the selected stations of the derived torsional component to the assumed torsional component, but in the case of table 1(a) these ratios are meaningless because the torsional component will ultimately be different than was assumed in column 1.

Before the results of further cycles of iteration for the first mode are described, the form that the numerical integration for the torsional component must take when GJ is variable is described. In the part of table 1(a) showing the calculation for variable GJ, columns 1 to 4 are the same as in the calculation for constant GJ. The form of the numerical integration changes at column 5. Column 5 consists of increments of twisting moment over the bays. These increments are obtained as increments of area beneath the curve of distributed torque (column 4). Formulas used for computing these increments are given in appendix C. In column 5 the increments of twisting moment are given in terms of the distances λ_i, and in column 6 they are given in terms of the reference distance λ_o. The twisting moments at the selected stations due to the distributed torsional loading are obtained in column 7 by a successive summation of the increments of twisting moment. The components of external concentrated torque are as for constant GJ and are given in columns 8 and 9. The applied concentrated torque gives twisting moments as shown in column 10. Column 11 is the sum of columns 7 and 10 and gives the total twisting moments at the selected stations. (Note that in columns 10 and 11 there is a discontinuity in twisting moment at the station having the mass discontinuity.) Column 12 gives the distribution of twist found by dividing column 11 by the local

value of GJ (GJ being in general not constant). The increments of derived torsional displacement are computed in columns 13 and 14 by applying to the values of column 12 the same formulas applied previously to column 4. The torsional component of the derived mode (columns 15 and 16) is, except for small computational discrepancies, the same as in the previous method, as it should be.

Two additional cycles of iteration were found to be adequate for the determination of the first mode and frequency. The results of these iterations are shown in parts (b) and (c) of table 1. In table 1(b), for example, columns 1 give the two components of the assumed mode of the second cycle, which are obtained by normalizing the derived mode of the first cycle to unity in the flexural component at the tip station. This normalization is not essential but facilitates manipulations and comparisons by keeping the numerical values in all cycles within the same range of magnitude. Columns 2 give the derived mode obtained by the numerical integration procedure just described. The ratios of derived to assumed mode are given in columns 3 for both components of displacement. These ratios are seen to be fairly uniform. The ratios obtained in the third cycle in table 1(c) are, for practical purposes, identical. The averaging device shown in columns 4 of table 1(c) and to the right of table 1(c) is adopted as a quick and generally quite accurate way of smoothing out small discrepancies that remain in the ratios after convergence is almost complete. This device, although clearly not necessary in the case of table 1(c), is useful in other cases throughout the numerical examples and is explained as follows: The two ratios in columns 4 are obtained by considering the flexural and torsional components of the displacement separately and then dividing the sum of the station values of the derived displacement by the sum of the station values of the assumed displacement. When a discrepancy remains between two ratios of the type in columns 4, the average of these two is taken as the final value; the final value for this case is given in the calculation to the right of table 1(c). This device gives greater weight to the larger ordinates and is in that respect similar to other weighting procedures such as the energy and least-squares methods but is much simpler. If the assumed and derived displacements contain both positive and negative ordinates, the negative ordinates should be changed to positive for the purpose of the summations. The remaining calculation shown to the right of table 1(c) gives that value of the arbitrary frequency ω which makes the ratio just computed unity. As proved in appendix A, this value of ω is the fundamental frequency ω_1.

Table 2 gives the main results of three cycles of iteration required to obtain satisfactory approximations of the second frequency and the transformed second mode at zero airspeed ($k = \infty$). Columns 1 of the first cycle (parts (a) of table 2) contain the two components $y_{a2}^{(1)}$ and $\phi_{a2}^{(1)}$ of the assumed transformed second mode. This mode must have

one zero ordinate (excluding the root ordinates). Although this zero ordinate may theoretically be taken at any station, the numerical accuracy of the results is greatest if the zero ordinate is placed at the station and in the component where the preceding mode (the first) has its maximum numerical value (since the numerical process is such that the larger ordinates contain more significant figures than the smaller ordinates). Therefore, the zero ordinate of the transformed second mode is placed at the tip station in the flexural component, this location being designated station A. In the numerical values of columns 1, the flexural component $y_{a2}^{(1)}$ would normally be taken as zero. (The values that are shown are estimated from flutter calculations that had previously been made for this wing.) Columns 2 give the intermediate derived mode obtained by numerical integration. Columns 3 constitute the first-mode sweeping function. The shape of this sweeping function is given by columns 2 of table 1(c) and its magnitude is such as to be equal and opposite to the intermediate derived mode at station A. Thus the derived transformed second mode (columns 4), which is the sum of columns 2 and 3, has zero ordinate in the flexural component at station A and a shape comparable to the assumed mode, as indicated by the ratios in columns 5. The ratios in the next two cycles (parts (b) and (c) of table 2) show marked improvement in uniformity. The final value of the ratio computed below the table gives, as proved in appendix A, the value of the second frequency ω_2, as shown.

The main results of the iterations to obtain satisfactory approximations of the third frequency and the transformed third mode at zero airspeed are stated in table 3. Typical operations required in a cycle are outlined in table 3(a). Columns 1 give the assumed transformed third mode made up of the two components $y_{a3}^{(1)}$ and $\phi_{a3}^{(1)}$. The transformed third mode is to have a zero ordinate in the flexural component at the tip station as in the transformed second mode and a zero ordinate in the torsional component at the tip station. The location of the second zero ordinate is designated station B. To obtain greatest numerical accuracy, the selection of the second zero ordinate is governed by the same rule that was used for selecting the first zero ordinate, namely, that the new zero ordinate should be placed at the station and in the component where the preceding mode (the transformed second) has its maximum numerical value. The numerical values that are shown in columns 1 are estimated from previous flutter calculations; the torsional component $\phi_{a3}^{(1)}$ would normally be taken as zero. Columns 2 give the intermediate derived mode, and columns 3 give the first-mode sweeping function which, as before, has a magnitude at station A that is equal and opposite to the intermediate derived mode. Columns 4 constitute the transformed-second-mode sweeping function which has a shape given by columns 4 of table 2(c) and a magnitude at station B equal and opposite

to the sum of the intermediate derived mode and the first-mode sweeping function (the sum of columns 2 and 3). The derived transformed third mode of the first cycle is the sum of columns 2, 3, and 4 and is given in columns 5. The ratios in columns 6 are far from uniform. The ratios in the second and third cycles (parts (b) and (c) of table 3) show improvements in uniformity. The iteration is discontinued at the end of the third cycle where the ratios are about as uniform as they can get with the limited number of significant figures that are present. The frequency obtained by the smoothing device is the third frequency ω_3 and has the value shown.

The patterns laid out in the foregoing examples establish the general technique that can be used to obtain zero-airspeed modes and frequencies higher than the third. Guiding rules for determining the number of selected stations to be employed have been given previously. These examples also set the basic pattern for the computation of the modes and eigenvalues of pseudoflutter and of flutter.

Modes and Eigenvalues of Pseudoflutter and of Flutter

The operational solution in reference 5 gave for the wing under consideration (fig. 3) a reduced frequency at flutter of 0.1443. In order to use this operational solution, this same value ($k = 0.1443$) is used in the flutter calculations that follow.

The calculations for the first, second, and third modes at $k = 0.1443$ are shown in tables 5, 6, and 7, respectively. Aerodynamic-inertia force coefficients have been computed by equations (19) to (35) and their values are given in table 4. Structural damping is disregarded, although a note on the method of incorporating structural damping in the calculations is made subsequently.

Table 5(a) shows in detail the first cycle of iteration for the first mode. The form of the computations is the same as that shown previously for the determination of zero-airspeed modes. The amount of computation, however, is between three and four times that required for zero-airspeed modes because of the fact that the functions involved are complex and thus must be described by two parts - a real part and an imaginary part. Columns 1 and 2 are the real and imaginary parts, respectively, of the assumed first mode. As a start, all parts of the assumed mode except the real part of the flexural component are taken as zero. Columns 3 to 6 are the real parts of the products of aerodynamic-inertia coefficients and the assumed mode, and thus their sums (columns 7) are the real parts of the distributed load. If the expressions for the distributed load are considered, this condition is more evident. The distributed forces producing flexure are given by

$$\left(P_{Ry} - iP_{Iy}\right)\left(y_R + iy_I\right) + \left(P_{R\phi} - iP_{I\phi}\right)\left(\phi_R + i\phi_I\right) = P_{Ry}y_R + P_{R\phi}\phi_R + P_{Iy}y_I + P_{I\phi}\phi_I + i\left(P_{Ry}y_I + P_{R\phi}\phi_I - P_{Iy}y_R - P_{I\phi}\phi_R\right) \quad (51)$$

The terms of the real part of equation (51) appear in columns 3 to 6 in the flexural part of table 5(a); the terms of the imaginary part of equation (51) appear in columns 22 to 25 in the flexural part of table 5(a). This separation of real and imaginary parts allows the displacement due to each part to be computed separately. A similar explanation can be made for the quantities in columns 3 to 6 and columns 18 to 21 in the torsional part of table 5(a).

Real and imaginary parts of the concentrated loads that are equivalent to the distributed loads are computed as explained previously by the formulas of appendix C. These values are shown in columns 8, 9, 27, and 28 in the flexural part and in columns 8, 9, 23, and 24 in the torsional part. The real and imaginary parts of the loads due to the concentrated mass follow next in order, and the total concentrated loads are given in columns 12 and 31 in the flexural part and in columns 12 and 27 in the torsional part. The average shears, average twisting moments, and bending moments are then computed as described previously.

The remaining parts of the computations in table 5(a) that are associated with the real parts of the load are described as follows (the remaining parts that are associated with the imaginary parts of the load are similar): Column 16 in the flexural part gives the distributed curvature due to the real part of the load. This curvature is obtained by dividing the ordinates of the real part of the bending-moment curve by the local values of the complex flexural stiffness $EI\left(1 + ig_y\right)\left(1 + ig_a\right)$. In these examples, any actual structural damping is disregarded; therefore g_y is zero. The factor $1 + ig_a$, containing the as yet unknown artificial-damping coefficient, combines with ω^2 to give the factor $1/C$ in column 16, C being the arbitrary eigenvalue $\frac{1 + ig_a}{\omega^2}$. If the actual structural damping g_y is regarded as other than zero, the values in column 16 would be computed as follows: The real and imaginary parts of the bending moment would be combined into the complex bending moment $M_R + iM_I$. This complex bending-moment distribution would then be divided by the local values of the complex stiffness to give $\frac{M_R + iM_I}{EI\left(1 + ig_y\right)\left(1 + ig_a\right)}$. The factor $1 + ig_a$ would be carried along in the arbitrary eigenvalue C, and the numerical values of the real part of the quotient $\frac{M_R + iM_I}{EI\left(1 + ig_y\right)}$

would be placed in column 16. The imaginary part of the quotient would be similarly placed (in column 35) in the calculations associated with the imaginary part of the load. The average twists due to the real part of the load are computed in column 14 in the torsional part of table 5(a), and those due to the imaginary part of the load must also be computed. These calculations follow the same pattern as those just explained for the curvatures. The complex torsional stiffness $GJ\left(1 + ig_{\phi}\right)\left(1 + ig_{a}\right)$ enters in place of the complex flexural stiffness. If GJ or g_{ϕ} is variable over a bay length or over the whole span, the numerical integration for the torsional part of the calculations should be carried out as explained in the part of table 1(a) that deals with variable GJ.

The numerical integrations are completed in the manner already described, and the derived mode is thereby obtained in the form of four components of displacement. The flexural components are $y_{1R}^{(2)}$ and $y_{1I}^{(2)}$ of columns 21 and 40 in the flexural part. The torsional components are $\phi_{1R}^{(2)}$ and $\phi_{1I}^{(2)}$ of columns 17 and 32 in the torsional part. However, these components are not actually the real and imaginary parts of the flexural and torsional components of the derived mode, because each one of them contains the complex factor $1 + ig_{a}$. Nevertheless, the complex derived mode is given by $y_{1R}^{(2)} + iy_{1I}^{(2)}$ and $\phi_{1R}^{(2)} + i\phi_{1I}^{(2)}$.

The complex ratios of the complex derived mode to the complex assumed mode are computed in column 41 in the flexural part and column 33 in the torsional part. Only two of these ratios have actually been computed but they are sufficient to indicate the need for further cycles of iteration.

A total of four cycles of iteration (the main results of the last three are shown in parts (b), (c), and (d) of table 5) were required for satisfactory convergence. In columns 6 of table 5(d) and immediately below table 5(d), the smoothing device described previously is applied to obtain the best single value of the ratios. The fundamental (first) eigenvalue is that value of C which makes the ratio unity. Thus $C_1 = \left(269.5 - 82.2i\right)\frac{\lambda_o^4 \gamma}{EI\mu}$, and since C_1 is defined as $\frac{1 + ig_{a1}}{\omega_1^2}$, the frequency and artificial damping of the first mode are obtained from the real and imaginary parts of the equation

$$\frac{1 + ig_{a1}}{\omega_1^2} = \left(269.5 - 82.2i\right)\frac{\lambda_o^4 \gamma}{EI\mu} \tag{52}$$

The calculation of these quantities and the corresponding airspeed v_1 which is obtained from the relation $v_1 = \frac{b\omega_1}{k}$ are shown at the bottom of table 5.

Tables 6 and 7 show the main results of the iterations to obtain the transformed second and third modes for $k = 0.1443$. Four cycles of iteration for each mode gave satisfactory convergence. The assumed modes of columns 1 and 2 of tables 6(a) and 7(a) were taken in the forms recommended previously in connection with tables 2 and 3. In tables 6 and 7, the complex intermediate derived modes are given by $y_{bR}^{(n)} + iy_{bI}^{(n)}$ and $\phi_{bR}^{(n)} + i\phi_{bI}^{(n)}$; the complex first-mode sweeping functions, by $y_{b1R}^{(n)} + iy_{b1I}^{(n)}$ and $\phi_{b1R}^{(n)} + i\phi_{b1I}^{(n)}$ with shapes corresponding to columns 3 and 4 of table 5(d); and the complex transformed-second-mode sweeping functions, by $y_{ba2R}^{(n)} + iy_{ba2I}^{(n)}$ and $\phi_{ba2R}^{(n)} + i\phi_{ba2I}^{(n)}$ with shapes corresponding to columns 7 and 8 of table 6(d). The results computed in and below table 7(d) give for the third eigenvalue, $g_{a3} = 0.030$ and $\omega_3 = 168.9$ radians per second. The corresponding airspeed is $v_3 = 390$ feet per second.

Computation of True Modes

Because the critical flutter velocities are given directly by the eigenvalues, knowledge of the true modes in flutter problems is of no value (at least of no value recognized at present). The same statement applies to the transformed pseudoflutter modes, with the exception that in the iterative method their determination is a necessary adjunct to the determination of the eigenvalues. In ordinary problems of forced vibration (at zero airspeed), however, the true modes are often used with great advantage. For this reason and for the sake of completeness of the presentation of the iterative transformation procedure, the method of determining true modes from results of the iterative transformation procedure is illustrated in tables 8 and 9.

The computations in tables 8 and 9 pertain to the same wing analyzed in the previous examples. The modes computed are for $k = 0.1443$. The true third mode as computed in table 9 may therefore be compared with the flutter mode computed for this wing by the operational method in reference 5.

In table 8, the true second mode is computed as follows from functions appearing in the last cycle of iteration for the transformed

second mode (table 6(d)): Preceding the table proper is the calculation of the eigenvalue factor $F_{12} = \frac{c_1}{c_2} - 1$ that is needed for computing the true second mode. In the terminology of tables 6(d) and 8 and as shown in appendix A, the true-second-mode shape is given by

$$y_{2R} + iy_{2I} = \left(y_{1R} + iy_{1I}\right) + \left(y^{(5)}_{a2R} + iy^{(5)}_{a2I}\right) \tag{53}$$

and

$$\phi_{2R} + i\phi_{2I} = \left(\phi_{1R} + i\phi_{1I}\right) + \left(\phi^{(5)}_{a2R} + i\phi^{(5)}_{a2I}\right) \tag{54}$$

in which

$$y_{1R} + iy_{1I} = \frac{y^{(4)}_{b1R} + iy^{(4)}_{b1I}}{\frac{c_1}{c_2} - 1} \tag{55}$$

and

$$\phi_{1R} + i\phi_{1I} = \frac{\phi^{(4)}_{b1R} + i\phi^{(4)}_{b1I}}{\frac{c_1}{c_2} - 1} \tag{56}$$

Columns 1 of table 8 show the key ordinate $\left(y^{(4)}_{b1R} + iy^{(4)}_{b1I}\right)_A$ of the first-mode sweeping function $y^{(4)}_{b1R} + iy^{(4)}_{b1I}$, $\phi^{(4)}_{b1R} + i\phi^{(4)}_{b1I}$ as given in columns 5 and 6 of table 6(d). The key ordinate is taken as the largest ordinate (the ordinate at station A) for the reason of accuracy cited previously. The key ordinate of the first-mode shape $y_{1R} + iy_{1I}$, $\phi_{1R} + i\phi_{1I}$ (equal to the first terms on the right-hand sides of equations (53) and (54)) is shown as the boxed value in column 2 and is obtained by dividing the value in column 1 by the eigenvalue factor F_{12}. The other values in columns 2 are obtained by using the key ordinate in conjunction with the first-mode shape given in columns 3 and 4 of table 5(d). Columns 3 show the transformed-second-mode shape $y^{(5)}_{a2R} + iy^{(5)}_{a2I}$, $\phi^{(5)}_{a2R} + i\phi^{(5)}_{a2I}$ (equal to the second terms on the right-hand

sides of equations (53) and (54)) given by columns 7 and 8 of table 6(d). The sum of columns 2 and 3 which is given in columns 4 gives the shape of the true second mode $y_{2R} + iy_{2I}$, $\phi_{2R} + i\phi_{2I}$ (equal to the left-hand sides of equations (53) and (54)).

In table 9, the computation of the true third mode proceeds as follows: The necessary eigenvalue factors $F_{13} = \frac{C_1}{C_3} - 1$ and $F_{23} = \frac{C_2}{C_3} - 1$ are computed as shown. In the terminology of tables 7(d) and 9 and as shown in appendix A, the true-third-mode shape is given by

$$y_{3R} + iy_{3I} = \left(y_{11R} + iy_{11I}\right) + \left(y_{12R} + iy_{12I}\right) + \left(y_{a2R} + iy_{a2I}\right) + \left(y^{(5)}_{a3R} + iy^{(5)}_{a3I}\right) \tag{57}$$

and

$$\phi_{3R} + i\phi_{3I} = \left(\phi_{11R} + i\phi_{11I}\right) + \left(\phi_{12R} + i\phi_{12I}\right) + \left(\phi_{a2R} + i\phi_{a2I}\right) + \left(\phi^{(5)}_{a3R} + \phi^{(5)}_{a3I}\right) \tag{58}$$

in which

$$\left(\frac{C_1}{C_3} - 1\right)\left(y_{11R} + iy_{11I}\right) + \left(\frac{C_2}{C_3} - 1\right)\left(y_{12R} + iy_{12I}\right) = y^{(4)}_{b1R} + iy^{(4)}_{b1I} \tag{59}$$

$$\left(\frac{C_1}{C_3} - 1\right)\left(\phi_{11R} + i\phi_{11I}\right) + \left(\frac{C_2}{C_3} - 1\right)\left(\phi_{12R} + i\phi_{12I}\right) = \phi^{(4)}_{b1R} + i\phi^{(4)}_{b1I} \tag{60}$$

$$y_{a2R} + iy_{a2I} = \frac{y^{(4)}_{ba2R} + iy^{(4)}_{ba2I}}{\frac{C_2}{C_3} - 1} \tag{61}$$

$$\phi_{a2R} + i\phi_{a2I} = \frac{\phi^{(4)}_{ba2R} + i\phi^{(4)}_{ba2I}}{\frac{C_2}{C_3} - 1} \tag{62}$$

and $y_{12R} + iy_{12I}$, $\phi_{12R} + i\phi_{12I}$ is to $y_{a2R} + iy_{a2I}$, $\phi_{a2R} + i\phi_{a2I}$ as $y_{1R} + iy_{1I}$, $\phi_{1R} + i\phi_{1I}$ is to $y^{(5)}_{a2R} + iy^{(5)}_{a2I}$, $\phi^{(5)}_{a2R} + i\phi^{(5)}_{a2I}$ in table 8. The key ordinates $\left(y^{(4)}_{b1R} + iy^{(4)}_{b1I}\right)_A$ and $\left(\phi^{(4)}_{ba2R} + i\phi^{(4)}_{ba2I}\right)_B$ of the first and second sweeping functions appear in columns 1 and 2 and are taken from columns 5, 6, 7, and 8 of table 7(d). The key ordinate of the functions $F_{23}\left(y_{12R} + iy_{12I}\right)$, $F_{23}\left(\phi_{12R} + i\phi_{12I}\right)$, which are equal to the second terms on the left-hand sides of equations (59) and (60), is computed in columns 3 by using the key ordinate of columns 2 in conjunction with ordinates at stations A and B in columns 2 and 3 of table 8 as follows:

$$\left[F_{23}\left(y_{12R} + iy_{12I}\right)_A\right]_{\text{table 9}} =$$

$$\left[\frac{\left(y_{1R} + iy_{1I}\right)_A}{\left(\phi^{(5)}_{a2R} + i\phi^{(5)}_{a2I}\right)_B}\right]_{\text{table 8}} \left[F_{23}\left(y_{a2R} + iy_{a2I}\right)_B\right]_{\text{table 9}} \tag{63}$$

The key ordinate of the functions $F_{13}\left(y_{11R} + iy_{11I}\right)$, $F_{13}\left(\phi_{11R} + i\phi_{11I}\right)$, which are equal to the first terms on the left-hand sides of equations (59) and (60), is given in columns 4 and, in accordance with equations (59) and (60), is the difference between $y^{(4)}_{b1R} + iy^{(4)}_{b1I}$, $\phi^{(4)}_{b1R} + i\phi^{(4)}_{b1I}$ of columns 1 and $F_{23}\left(y_{12R} + iy_{12I}\right)$, $F_{23}\left(\phi_{12R} + i\phi_{12I}\right)$ of columns 3. The key ordinates of the first-mode shapes $y_{11R} + iy_{11I}$, $\phi_{11R} + i\phi_{11I}$ and $y_{12R} + iy_{12I}$, $\phi_{12R} + i\phi_{12I}$ are shown in columns 6 and 5 and are obtained by dividing the values in columns 3 and 4 by the appropriate eigenvalue factors. The sum of the key ordinates of columns 5 and 6, shown as the boxed value in column 7, is the key ordinate of the total-first-mode shape $y_{1R} + iy_{1I}$, $\phi_{1R} + i\phi_{1I}$ which is equal to the sums of the first two terms on the right-hand sides of equations (57) and (58). The other values in columns 7 are obtained by using the key ordinate in conjunction with the first-mode shape given in columns 3 and 4 of table 5(d). The key ordinate of the transformed-second-mode shape $y_{a2R} + iy_{a2I}$, $\phi_{a2R} + i\phi_{a2I}$, which is equal to the third terms on the right-hand sides of equations (57) and (58), is shown as the boxed value in columns 8 and

is obtained by dividing the value in columns 2 by the eigenvalue factor F_{23}. The other values in columns 8 are computed by using the key ordinate in conjunction with the transformed-second-mode shape given in columns 7 and 8 of table 6(d). Columns 9 show the transformed-third-mode shape $y^{(5)}_{a3R} + iy^{(5)}_{a3I}$, $\phi^{(5)}_{a3R} + i\phi^{(5)}_{a3I}$ (equal to the fourth terms on the right-hand sides of equations (57) and (58)) given by columns 9 and 10 of table 7(d). The sum of columns 7, 8, and 9 given in columns 10 gives the shape of the true third mode $y_{3R} + iy_{3I}$, $\phi_{3R} + i\phi_{3I}$ (equal to the left-hand sides of equations (57) and (58)).

DISCUSSION OF RESULTS

Trends and Comparisons of Numerical Results

Results of the computations shown in the preceding section of the paper together with results of similar computations based on other assumed values of k are given in figures 4 to 6. Figures 4 and 5 deal with the wing to which the concentrated mass is attached. Figure 6 gives data of a similar nature for the same wing without the concentrated mass. The computed results obtained by the Rayleigh-Ritz and operational methods and the experimental results, all of which are given for this wing in references 5 and 6, are also recorded in figures 4 to 6.

In part (a) of figure 4 the solid curves show the variation of the artificial-damping coefficient g_a with airspeed in each of the first three solutions. For each assumed value of k a dashed curve is drawn through points that represent solutions for that value of k. Part (b) of figure 4 shows in a similar way the variation of the frequency ω with airspeed and the lines of constant values of k. The facts of particular interest that are shown by these plots are as follows:

(1) The true flutter condition is given by the third solution for a value of k between 0.1443 and 0.1590 at an airspeed almost equal to that found in the experiment. Here the computed value of g_a is zero. The computed frequency at true flutter is also in very close agreement with the experimental value.

(2) The operational solution is in good agreement with the experimental solution, but the solutions obtained by the Rayleigh-Ritz method with three and four modes vary by 72 percent and 22 percent, respectively, from the solution obtained by the operational method. The operational solution is theoretically the most exact even though it involves summations of finite numbers of terms of infinite series. However, as pointed out in reference 5, its use is limited in practice to wings of uniform

section. In the present example the results obtained by the iterative method would be expected to be better than the results obtained by the Rayleigh-Ritz method because the eight degrees of freedom used in the iterative method are much less restrictive than the three or four used in the Rayleigh-Ritz method. Although exact agreement of the results of any of the computational methods with the experimental results is not to be expected, the better agreement of the iterative solution as compared with the operational solution is at first surprising. On further observation, however, this agreement must be credited to a fortunate disposition of the errors involved in the iterative method because, in the case of figure 6, the relative order of agreement of the operational and iterative results with the experimental result is opposite to that in figure 4.

(3) The trends of the solid curves representing the first and second solutions in figure 4(a) indicate that both may cross the zero artificial-damping axis at very large airspeeds. But this conjecture is of no practical interest so long as a curve (the third solution) that crosses at a lower airspeed exists. However, the question of whether the curve for some solution higher than the third could cross the zero artificial-damping axis at an airspeed lower than that at which the third solution crosses demands an answer.

(4) Reasonable assurance that, among all possible solutions, the curve of third solutions in figure 4(a) crosses the zero artificial-damping axis at a lower airspeed than any other is provided by the trends of the curves for constant values of k in parts (a) and (b) of figure 4. The curves of k show that the curves representing the fourth solution will most assuredly lie above and to the right of the solid curves in figure 4(b) and probably below and to the right of the solid curve for the third solution in figure 4(a). The curves of k in figure 4(b) are straight lines by definition $\left(k = \frac{b\omega}{v}\right)$. Prediction of the courses of the curves of k in figure 4(a) cannot be made with much certainty. They have a strong tendency to proceed to the right, but it is easy to believe that upward or downward changes in their directions could take place. The curve for the fourth solution, however, would probably cross the zero damping axis at a value of v between 500 and 600 feet per second in figure 4(a).

Figure 5 shows and compares the amplitude and phase distributions of modes computed by the iterative transformation procedure and by the operational method for the wing with a concentrated mass. The first and second modes as well as the more important third mode from the iterative solution for $k = 0.1443$ are plotted, and the third mode from the iterative solution for $k = 0.1590$ is also plotted. The third modes from the iterative solutions for the two values of k agree very well in shape with the flutter mode obtained in reference 5 by the operational

method, and the operational mode lies between the two iterative modes. Thus the agreement of the iterative and the operational methods is again evidenced.

Figure 6 is a plot similar to figure 4 but relates to the behavior of the wing analyzed in figure 4 if the concentrated mass is not present. There is very little similarity in the data of the two figures. The most notable difference is that in figure 6 the true flutter mode appears in the second solution instead of the third as before and that the flutter speed is lower than before. Of interest is the occurrence of almost equal eigenvalues in the second and third solutions for $k = 0.50$. The flutter speeds given in figure 6 by all methods of solution, including the Rayleigh-Ritz method, are seen to be in substantial agreement.

CONCLUDING REMARKS

The paper has described the iterative transformation method suggested by H. Wielandt and has demonstrated the use of the method in an orderly computation of critical flutter speeds. Numerical comparisons with solutions obtained by other methods and with experimental values have been made. The applications made in this paper show promise for future practical use of the method.

Langley Aeronautical Laboratory
National Advisory Committee for Aeronautics
Langley Field, Va., January 17, 1951

APPENDIX A

ON THE CONVERGENCE OF THE ITERATIVE TRANSFORMATION PROCEDURE

Introduction

The extensive existing literature on the eigenvalue problems is concerned almost exclusively with the class known as self-adjoint problems, in which the eigenfunctions and eigenvalues are real. In recent years, non-self-adjoint eigenvalue problems have received increasing attention. This class includes the flutter problem in which the eigenfunctions and eigenvalues are generally complex. The literature referred to by Wielandt in reference 3 reveals that the non-self-adjoint eigenvalue problem and the transformation method for its solution have been given some attention since at least 1928. Wielandt's own work constitutes probably the most extensive contribution on the subject.

The discussion on convergence given herein is not contained in Wielandt's work and may be considered a rigorous proof if the following assumption is valid: that the equations (equations (41) and (42)) for the system (the wing) under consideration have an infinite number of solutions that form a complete set for any value of the reduced frequency k. In the subsequent demonstrations, the validity of expanding arbitrary displacement functions in infinite series of eigenfunctions depends upon the validity of the assumption. That complete sets of eigenfunctions do exist seems plausible enough to justify reliance in the conclusions.

Basic Relations

For any one of the true solutions of the eigenvalue problem, for example, the eigenvalue C_m and eigenfunction y_m, ϕ_m, equations (41) and (42) may be written as

$$C_m y_m = \int_0^x \int_0^x \frac{1}{EI\left(1 + ig_y\right)} \int_x^L \int_x^L \left(P_y' y_m + P_\phi' \phi_m\right)(dx)^4 \qquad (A1)$$

and

$$C_m \phi_m = \int_0^x \frac{1}{GJ\left(1 + ig_\phi\right)} \int_x^L \left(Q_y' y_m + Q_\phi' \phi_m\right)(dx)^2 \qquad (A2)$$

To make the notation more concise, let the coupled mode y_m,ϕ_m be represented by w_m. Then if y_m,ϕ_m is substituted into the right-hand sides of equations (A1) and (A2), the left-hand sides may be represented by $C_m w_m$. Furthermore, because of the linear character of the equations of the problem, substitution of the function series

$$\sum_{i=1}^{\infty} a_i w_i \tag{A3}$$

into the right-hand sides of equations (A1) and (A2) gives for the left-hand sides the function series

$$\sum_{i=1}^{\infty} C_i a_i w_i \tag{A4}$$

The coefficients a_i are, in general, complex. The complex eigenvalues C_i are assumed in the subsequent proofs, except where stated otherwise, to be different from each other, and the eigenvalue having the largest modulus is defined as C_1, the second largest, as C_2, and so forth, so that

$$\left|C_1\right| > \left|C_2\right| > \left|C_3\right| > \cdots \tag{A5}$$

Expressions (A3) and (A4) are the expansions, in terms of the eigenfunctions and the eigenvalues, of the functions previously referred to as the assumed and intermediate derived modes, respectively. The subsequent proofs of convergence are based upon the fundamental relationship that exists between expressions (A3) and (A4).

Fundamental Mode

The fundamental mode and eigenvalue are found by iteration according to the original Stodola procedure. In the present terminology and notation, this procedure and its proof of convergence are as follows: The coupled mode assumed at the beginning of the first cycle of iteration in general contains some component of each of the eigenfunctions; therefore its most general expression is

$$w_1^{(1)} = \sum_{i=1}^{\infty} a_i w_i \tag{A6}$$

The intermediate derived mode (which in this case is also the final derived mode inasmuch as no sweeping operation is required to obtain the first mode) is for this first cycle of iteration

$$w_b^{(1)} \equiv w_1^{(2)} = \sum_{i=1}^{\infty} C_i a_i w_i \tag{A7}$$

The second and following cycles are begun with the final derived mode of each preceding cycle, and thus the assumed and derived modes of the nth cycle are

$$w_1^{(n)} = \sum_{i=1}^{\infty} C_i^{n-1} a_i w_i \tag{A8}$$

$$w_1^{(n+1)} = \sum_{i=1}^{\infty} C_i^{n} a_i w_i \tag{A9}$$

In accordance with the definitions given in equation (A5), all terms on the right-hand sides of equations (A8) and (A9) except the first are negligibly small in comparison with the first for large values of n. In the limit the fundamental mode is obtained as

$$\lim_{n \to \infty} w_1^{(n+1)} = \lim_{n \to \infty} C_1^{n} a_1 w_1 \tag{A10}$$

and the fundamental eigenvalue is obtained from

$$\lim_{n \to \infty} \frac{w_1^{(n+1)}}{w_1^{(n)}} = C_1 \tag{A11}$$

Transformed Second Mode

The initial assumption of the transformed second mode in general is of the form

$$w_{a2}^{(1)} = \sum_{i=2}^{\infty} b_i \left[w_i - \left(\frac{w_i}{w_1} \right)_A w_1 \right] \tag{A12}$$

in which the arbitrary coefficients b_i are in general complex and the subscript A refers to values of either the flexural or torsional components of the eigenfunctions at station A. More specifically, if, for example, the nodal (zero) point of w_{a2} is selected to be at station A in the flexural component, then the subscript A refers only to the flexural components of w_1, w_2, w_3, . . . and not to their torsional components. Thus each term of the series in equation (A12) satisfies the requirement that either the flexural or torsional component of the assumed mode be zero at station A.

To simplify the subsequent work as much as possible, the eigenfunctions are henceforth assumed to be normalized to unity at station A; thus

$$\left(w_i\right)_A = 1 \qquad (i = 1, 2, 3, \ldots) \tag{A13}$$

Equation (A12) now takes the simpler form

$$w_{a2}^{(1)} = \sum_{i=2}^{\infty} b_i \left(w_i - w_1\right) \tag{A14}$$

The assumed mode given by equation (A14) leads, according to equations (A3) and (A4), to the following intermediate derived mode:

$$w_b^{(1)} = \sum_{i=2}^{\infty} b_i \left(C_i w_i - C_1 w_1\right) \tag{A15}$$

Sweeping of this intermediate derived mode with the first-mode shape (previously determined) leads to the derived transformed second mode of the first cycle as follows:

$$w_{a2}^{(2)} = w_b^{(1)} - \left(\frac{w_b^{(1)}}{w_1}\right)_A w_1 = \sum_{i=2}^{\infty} C_i b_i \left(w_i - w_1\right) \tag{A16}$$

When each succeeding cycle is begun with the derived transformed second mode of its preceding cycle, the various functions for the nth cycle are

$$w_{a2}^{(n)} = \sum_{i=2}^{\infty} C_i^{\,n-1} b_i \left(w_i - w_1\right) \tag{A17}$$

$$w_b^{(n)} = \sum_{i=2}^{\infty} C_i^{n-1} b_i \left(C_i w_i - C_1 w_1\right) \tag{A18}$$

$$w_{a2}^{(n+1)} = \sum_{i=2}^{\infty} C_i^{n} b_i \left(w_i - w_1\right) \tag{A19}$$

The limits as n approaches infinity are

$$\lim_{n \to \infty} w_{a2}^{(n+1)} = \lim_{n \to \infty} C_2^{n} b_2 \left(w_2 - w_1\right) \tag{A20}$$

and

$$\lim_{n \to \infty} \frac{w_{a2}^{(n+1)}}{w_{a2}^{(n)}} = C_2 \tag{A21}$$

Equations (A20) and (A21) show that convergence to the exact-transformed-second-mode shape $w_2 - w_1$ and to the exact second eigenvalue C_2 can be obtained theoretically.

True Second Mode

The key to computation of the true second mode is readily found in the simple case illustrated in figure 1. In this case the sweeping function of the final cycle of iteration would be the displacement produced by the forcing load $\gamma\left(\omega_2^2 - \omega_1^2\right)y_1$, in which y_1 is the first-mode component of the transformed second mode y_{a2}. The sweeping function is designated by y_{b1} which has a well-defined numerical value in the iteration. Thus the value of y_1 could be found from the equation

$$y_{b1} = \frac{\gamma\left(\omega_2^2 - \omega_1^2\right)y_1}{\gamma\omega_1^2} = \left(\frac{\omega_2^2}{\omega_1^2} - 1\right)y_1 \tag{A22}$$

that is,

$$y_1 = \frac{y_{b1}}{\frac{\omega_2^2}{\omega_1^2} - 1} \tag{A23}$$

The sum of y_{a2} given in the iteration and y_1 given by equation (A23) gives y_2, the true second mode; that is,

$$y_{a2} + y_1 = y_2 - y_1 + y_1 = y_2 \tag{A24}$$

By analogy, the true-second-mode shape in the general (complex) problem under consideration is found as follows: The limiting value of the sweeping function is, from equation (A18),

$$\lim_{n\to\infty} w_{b1}^{(n)} = \lim_{n\to\infty} \left(\frac{-w_b^{(n)}}{w_1}\right)_A w_1 = \lim_{n\to\infty} C_2^n \left(\frac{C_1}{C_2} - 1\right) b_2 w_1 \tag{A25}$$

The expression analogous to equation (A23) is

$$\frac{\lim_{n\to\infty} w_{b1}^{(n)}}{\frac{C_1}{C_2} - 1} = \lim_{n\to\infty} C_2^n b_2 w_1 \tag{A26}$$

The expression analogous to equation (A24) is

$$\lim_{n\to\infty} w_{a2}^{(n+1)} + \frac{\lim_{n\to\infty} w_{b1}^{(n)}}{\frac{C_1}{C_2} - 1} = \lim_{n\to\infty} C_2^n b_2 w_2 \tag{A27}$$

which gives the exact shape of the true second mode.

Transformed Third Mode

The first cycle of iteration for the transformed third mode begins with an assumed mode that has two zero values, one of these being in the same (flexural or torsional) component and at the same station (station A) as previously employed for the transformed second mode. The other zero value may be taken in the same component as was the first

zero value and at a different station (station B), or it may be taken in the other component at any station, including station A. Either of these possible selections for the location of the second zero value is indicated in the following equations by use of the subscript B. The initially assumed transformed third mode may be written as

$$w_{a3}^{(1)} = \sum_{i=3}^{\infty} d_i \left[w_i - w_1 - \left(\frac{w_i - w_1}{w_2 - w_1} \right)_B \left(w_2 - w_1 \right) \right] \tag{A28}$$

in which the arbitrary coefficients d_i are complex. Each term of the series in equation (A28) is zero at station A by reason of the normalizations stated in equation (A13), and each term is also zero at station B.

The various displacement functions for the general (nth) cycle of iteration may be expressed as follows: The assumed mode is

$$w_{a3}^{(n)} = \sum_{i=3}^{\infty} C_i^{n-1} d_i \left[w_i - w_1 - \left(\frac{w_i - w_1}{w_2 - w_1} \right)_B \left(w_2 - w_1 \right) \right] \tag{A29}$$

The intermediate derived mode is

$$w_b^{(n)} = \sum_{i=3}^{\infty} C_i^{n-1} d_i \left[C_i w_i - C_1 w_1 - \left(\frac{w_i - w_1}{w_2 - w_1} \right)_B \left(C_2 w_2 - C_1 w_1 \right) \right] \tag{A30}$$

The result after sweeping the intermediate derived mode with a first-mode shape such as to make the sum zero at station A is as follows:

$$w_b^{(n)} - \left(\frac{w_b^{(n)}}{w_1} \right)_A w_1 = \sum_{i=3}^{\infty} C_i^{n-1} d_i \left[C_i \left(w_i - w_1 \right) - \left(\frac{w_i - w_1}{w_2 - w_1} \right)_B C_2 \left(w_2 - w_1 \right) \right] \tag{A31}$$

Sweeping of the mode given by equation (A31) with a transformed-second-mode shape such as to make the sum zero in the flexural or torsional component (as the case may be) at station B gives the derived transformed third mode as follows:

$$w_{a3}^{(n+1)} = w_b^{(n)} - \left(\frac{w_b^{(n)}}{w_1}\right)_A w_1 - \left[\frac{w_b^{(n)} - \left(\frac{w_b^{(n)}}{w_1}\right)_A w_1}{w_2 - w_1}\right]_B (w_2 - w_1)$$

$$= \sum_{i=3}^{\infty} C_i^n d_i \left[w_i - w_1 - \left(\frac{w_i - w_1}{w_2 - w_1}\right)_B (w_2 - w_1)\right] \quad (A32)$$

The limits as n approaches infinity are

$$\lim_{n\to\infty} w_{a3}^{(n+1)} = \lim_{n\to\infty} C_3^n d_3 \left[w_3 - w_1 - \left(\frac{w_3 - w_1}{w_2 - w_1}\right)_B (w_2 - w_1)\right] \quad (A33)$$

and

$$\lim_{n\to\infty} \frac{w_{a3}^{(n+1)}}{w_{a3}^{(n)}} = C_3 \quad (A34)$$

As shown by equations (A33) and (A34), convergence to the exact-transformed-third-mode shape $w_3 - w_1 - \left(\frac{w_3 - w_1}{w_2 - w_1}\right)_B (w_2 - w_1)$ and to the exact third eigenvalue C_3 can be obtained theoretically.

True Third Mode

Computation of the true third mode is explained by referring again to the simple problem of pure flexural vibration in which air forces are excluded. The transformed third mode in this simple problem would be given by

$$y_{a3} = y_3 - y_1 - \left(\frac{y_3 - y_1}{y_2 - y_1}\right)_B (y_2 - y_1) \quad (A35)$$

The total load required to hold the beam in equilibrium in the shape y_{a3} is

$$\gamma\omega_3^2 y_3 - \gamma\omega_1^2\left[1 - \left(\frac{y_3 - y_1}{y_2 - y_1}\right)_B\right]y_1 - \gamma\omega_2^2\left(\frac{y_3 - y_1}{y_2 - y_1}\right)_B y_2 \tag{A36}$$

If the beam is vibrating with shape y_{a3} at frequency ω_3, the inertia load is given by

$$\gamma\omega_3^2 y_{a3} = \gamma\omega_3^2\left[y_3 - y_1 - \left(\frac{y_3 - y_1}{y_2 - y_1}\right)_B\left(y_2 - y_1\right)\right] \tag{A37}$$

The forcing load required is the difference between the total load (expression (A36)) and the inertia load (equation (A37)), that is,

$$\gamma\left(\omega_3^2 - \omega_1^2\right)\left[1 - \left(\frac{y_3 - y_1}{y_2 - y_1}\right)_B\right]y_1 + \gamma\left(\omega_3^2 - \omega_2^2\right)\left(\frac{y_3 - y_1}{y_2 - y_1}\right)_B y_2 \tag{A38}$$

The displacement produced by this forcing load is

$$\left(\frac{\omega_3^2}{\omega_1^2} - 1\right)\left[1 - \left(\frac{y_3 - y_1}{y_2 - y_1}\right)_B\right]y_1 + \left(\frac{\omega_3^2}{\omega_2^2} - 1\right)\left(\frac{y_3 - y_1}{y_2 - y_1}\right)_B y_2 \tag{A39}$$

and this displacement must be equal to the sum of the sweeping functions in the last cycle of iteration (if the iteration has been carried to complete convergence). The first sweeping function is of the first-mode shape and the second sweeping function is of the transformed-second-mode shape. If the expression (A39) is written in the form

$$\left(\frac{\omega_3^2}{\omega_1^2} - 1\right)\left[1 - \left(\frac{y_3 - y_1}{y_2 - y_1}\right)_B\right]y_1 + \left(\frac{\omega_3^2}{\omega_2^2} - 1\right)\left(\frac{y_3 - y_1}{y_2 - y_1}\right)_B y_1 +$$

$$\left(\frac{\omega_3^2}{\omega_2^2} - 1\right)\left(\frac{y_3 - y_1}{y_2 - y_1}\right)_B\left(y_2 - y_1\right) \tag{A40}$$

each of the sweeping functions contained in the displacement produced by the forcing load is obvious. Thus

$$y_{b1} = \left(\frac{\omega_3^2}{\omega_1^2} - 1\right)\left[1 - \left(\frac{y_3 - y_1}{y_2 - y_1}\right)_B\right]y_1 + \left(\frac{\omega_3^2}{\omega_2^2} - 1\right)\left(\frac{y_3 - y_1}{y_2 - y_1}\right)_B y_1 \tag{A41}$$

and

$$y_{ba2} = \left(\frac{\omega_3^2}{\omega_2^2} - 1\right)\left(\frac{y_3 - y_1}{y_2 - y_1}\right)_B (y_2 - y_1) \tag{A42}$$

in which y_{b1} and y_{ba2} designate the first and second sweeping functions, respectively. Both of these functions have well-defined numerical values in the iteration.

If now a simpler notation is adopted, equations (A41) and (A42) can be written as

$$y_{b1} = \left(\frac{\omega_3^2}{\omega_1^2} - 1\right)y_{11} + \left(\frac{\omega_3^2}{\omega_2^2} - 1\right)y_{12} \tag{A43}$$

and

$$y_{ba2} = \left(\frac{\omega_3^2}{\omega_2^2} - 1\right)y_{a2} \tag{A44}$$

in which

$$y_{11} = \left[1 - \left(\frac{y_3 - y_1}{y_2 - y_1}\right)_B\right]y_1 \tag{A45}$$

$$y_{12} = \left(\frac{y_3 - y_1}{y_2 - y_1}\right)_B y_1 \tag{A46}$$

and

$$y_{a2} = \left(\frac{y_3 - y_1}{y_2 - y_1}\right)_B \left(y_2 - y_1\right) \tag{A47}$$

The true third mode is clearly given by the sum of equations (A35), (A45), (A46), and (A47); thus

$$y_3 = y_{a3} + y_{11} + y_{12} + y_{a2} \tag{A48}$$

The transformed third mode y_{a3} is given directly in the iteration. The procedure for finding the other components on the right-hand side of equation (A48) is as follows: Component y_{a2}, by equation (A44), is

$$y_{a2} = \frac{y_{ba2}}{\frac{\omega_3^2}{\omega_2^2} - 1} \tag{A49}$$

Component y_{12} is known when y_{a2} is known because its relation to y_{a2} was established previously in connection with the transformed-second-mode calculations (see equation (A24)). Component y_{11} is then found by equation (A43) as

$$y_{11} = \frac{y_{b1} - \left(\frac{\omega_3^2}{\omega_2^2} - 1\right) y_{12}}{\frac{\omega_3^2}{\omega_1^2} - 1} \tag{A50}$$

By analogy with the foregoing case, the true third mode in the complex-eigenvalue problem is found as follows: The limiting value of the second sweeping function is (see equations (A31) and (A32))

$$\lim_{n\to\infty} w_{ba2}^{(n)} = -\lim_{n\to\infty}\left[\frac{w_b^{(n)} - \left(\frac{w_b^{(n)}}{w_1}\right)_A w_1}{w_2 - w_1}\right]_B (w_2 - w_1)$$

$$= \lim_{n\to\infty} C_3{}^n\left(\frac{C_2}{C_3} - 1\right) d_3 \left(\frac{w_3 - w_1}{w_2 - w_1}\right)_B (w_2 - w_1) \qquad (A51)$$

The limiting value of the first sweeping function is (see equations (A30) and (A31))

$$\lim_{n\to\infty} w_{b1}^{(n)} = -\lim_{n\to\infty}\left(\frac{w_b^{(n)}}{w_1}\right)_A w_1$$

$$= \lim_{n\to\infty} C_3{}^n d_3\left[\frac{C_1}{C_3} - 1 - \left(\frac{C_1}{C_3} - \frac{C_2}{C_3}\right)\left(\frac{w_3 - w_1}{w_2 - w_1}\right)_B\right] w_1 \qquad (A52)$$

The quantities analogous to y_{12} and y_{a2} of equations (A43) and (A44) are, for the present case, $\lim_{n\to\infty} w_{12}^{(n)}$ and $\lim_{n\to\infty} w_{a2}^{(n)}$. The latter quantity is obtained from the relation analogous to equation (A49) as follows:

$$\lim_{n\to\infty} w_{a2}^{(n)} = \frac{\lim_{n\to\infty} w_{ba2}^{(n)}}{\frac{C_2}{C_3} - 1} = \lim_{n\to\infty} C_3{}^n d_3 \left(\frac{w_3 - w_1}{w_2 - w_1}\right)_B (w_2 - w_1) \qquad (A53)$$

The relationship of $\lim_{n\to\infty} w_{12}^{(n)}$ and $\lim_{n\to\infty} w_{a2}^{(n)}$ is obtained from equations (A26) and (A20) of the section dealing with the transformed second mode. Thus,

$$\lim_{n\to\infty} w_{12}^{(n)} = \lim_{n\to\infty} \frac{\left[\left(w_{a2}^{(n)}\right)_B\right]_{\text{Eq.(A53)}}}{\left[\left(w_{a2}^{(n+1)}\right)_B\right]_{\text{Eq.(A20)}}} \left[\frac{\lim_{n\to\infty} w_{b1}^{(n)}}{\frac{C_1}{C_2} - 1}\right]_{\text{Eq.(A26)}}$$

$$= \lim_{n\to\infty} C_3^{\,n} d_3 \left(\frac{w_3 - w_1}{w_2 - w_1}\right)_B w_1 \tag{A54}$$

The quantity analogous to y_{11} of equation (A43) is, for the present case, $\lim_{n\to\infty} w_{11}^{(n)}$ and is obtained by an equation analogous to equation (A50) as follows:

$$\lim_{n\to\infty} w_{11}^{(n)} = \frac{\lim_{n\to\infty} w_{b1}^{(n)} - \left(\frac{C_2}{C_3} - 1\right) \lim_{n\to\infty} w_{12}^{(n)}}{\frac{C_1}{C_3} - 1}$$

$$= \lim_{n\to\infty} C_3^{\,n} d_3 \left[1 - \left(\frac{w_3 - w_1}{w_2 - w_1}\right)_B\right] w_1 \tag{A55}$$

The exact shape of the true third mode w_3 is given by the sum of equations (A33), (A53), (A54), and (A55), which is

$$\lim_{n\to\infty} \left(w_{a3}^{(n+1)} + w_{a2}^{(n)} + w_{11}^{(n)} + w_{12}^{(n)}\right) = \lim_{n\to\infty} C_3^{\,n} d_3 w_3 \tag{A56}$$

Fourth and Higher Modes

Extensions of the proofs to modes higher than the third can be made in a manner similar to the foregoing proofs. By this means, the iterative transformation procedure can be proved, under the assumptions stated at the beginning of this appendix, to be convergent for all modes and eigenvalues.

Cases of Eigenvalues Having Equal or Nearly Equal Moduli

For a representative case, suppose that

$$|c_1| > |c_2|; \qquad |c_3| > |c_4| > \cdots \tag{A57}$$

and that

$$|c_2| = |c_3| \tag{A58}$$

or that

$$|c_2| \approx |c_3| \tag{A59}$$

Under conditions (A57) and either (A58) or (A59), the assumed and derived modes after a few cycles of iteration will be virtually as follows (see equations (A17) and (A19)):

$$w_{a2}^{(n)} = c_2^{n-1} b_2 (w_2 - w_1) + c_3^{n-1} b_3 (w_3 - w_1) \tag{A60}$$

$$w_{a2}^{(n+1)} = c_2^{n} b_2 (w_2 - w_1) + c_3^{n} b_3 (w_3 - w_1) \tag{A61}$$

If $|c_2|$ is only slightly greater than $|c_3|$, the second terms on the right-hand sides of equations (A60) and (A61) become negligibly small very slowly as n increases, even though they do become negligibly small as n approaches infinity. If $|c_2|$ and $|c_3|$ are equal, these terms never become negligibly small. Thus, the problem of circumventing this slow convergence or apparent lack of convergence arises.

A satisfactory method for coping with these conditions is to combine linearly the results of the last two cycles of the series of iteration cycles that have been performed. For best results in an actual problem, not less than the third and fourth cycles should be used for this purpose in order to reduce as much as practicable the effects of all higher-order components.

The following formulas for combining the results of the last two cycles are based on the assumption that the assumed and derived modes in each of the cycles contain only components of the types in equations (A60) and (A61).

The two components (with shapes $w_2 - w_1$ and $w_3 - w_1$) clearly appear in the last cycle in proportions different than in the preceding cycle. (The proportion in each cycle is a complex function of the spanwise coordinate.) Because of this differing proportionality the results of cycles $n - 1$ and n can be linearly combined so that the combined functions contain only one of the components $w_2 - w_1$ and $w_3 - w_1$. Accordingly, the ratios of both the flexural and torsional components of the combined functions at all stations should be equal to each other. In algebraic terms, this statement means that

$$\left(\frac{r w_{a2}^{(n)} + w_{a2}^{(n+1)}}{r w_{a2}^{(n-1)} + w_{a2}^{(n)}} \right)_S = R \tag{A62}$$

in which r and R are (complex) constants, and the subscript S designates that the ratio may be evaluated at any station S, that is, that R has the same value for all stations. All w functions must be the same type of component, either flexural or torsional.

Since S can be any station, the equality

$$\left(\frac{r w_{a2}^{(n)} + w_{a2}^{(n+1)}}{r w_{a2}^{(n-1)} + w_{a2}^{(n)}} \right)_1 = \left(\frac{r w_{a2}^{(n)} + w_{a2}^{(n+1)}}{r w_{a2}^{(n-1)} + w_{a2}^{(n)}} \right)_2 \tag{A63}$$

exists, in which stations 1 and 2 must be different or may be the same, depending on whether the w functions on the left-hand side are the same or different types of components than those on the right-hand side. The two values of r that satisfy equation (A63) are

$$r = - \frac{A^{(n-1),(n+1)}}{A^{(n-1),(n)}} \pm \sqrt{\left(\frac{A^{(n-1),(n+1)}}{A^{(n-1),(n)}} \right)^2 - \frac{A^{(n),(n+1)}}{A^{(n-1),(n)}}} \tag{A64}$$

in which

$$A^{(n-1),(n)} = \begin{vmatrix} \left(w_{a2}^{(n-1)}\right)_1 & \left(w_{a2}^{(n-1)}\right)_2 \\ \left(w_{a2}^{(n)}\right)_1 & \left(w_{a2}^{(n)}\right)_2 \end{vmatrix} \tag{A65}$$

$$A^{(n),(n+1)} = \begin{vmatrix} \left(w_{a2}^{(n)}\right)_1 & \left(w_{a2}^{(n)}\right)_2 \\ \left(w_{a2}^{(n+1)}\right)_1 & \left(w_{a2}^{(n+1)}\right)_2 \end{vmatrix} \tag{A66}$$

$$A^{(n-1),(n+1)} = \begin{vmatrix} \left(w_{a2}^{(n-1)}\right)_1 & \left(w_{a2}^{(n-1)}\right)_2 \\ \left(w_{a2}^{(n+1)}\right)_1 & \left(w_{a2}^{(n+1)}\right)_2 \end{vmatrix} \tag{A67}$$

The corresponding values of R are

$$R = \frac{A^{(n-1),(n+1)}}{A^{(n-1),(n)}} \pm \sqrt{\left(\frac{A^{(n-1),(n+1)}}{A^{(n-1),(n)}}\right)^2 - \frac{A^{(n),(n+1)}}{A^{(n-1),(n)}}}$$

$$= -\frac{A^{(n),(n+1)} \Big/ A^{(n-1),(n)}}{r} \tag{A68}$$

These values of R are equal to C_2 and C_3, and the corresponding values of r, when placed in the expression

$$r w_{a2}^{(n)} + w_{a2}^{(n+1)} \tag{A69}$$

give modes of the shapes $w_2 - w_1$ and $w_3 - w_1$. When $|C_2|$ is nearly equal to $|C_3|$, the appropriate set of R and r to give the lower transformed mode $w_2 - w_1$ is evident. When $|C_2|$ and $|C_3|$ are equal, the mode obtained by equation (A69) with either value of r may be used as the transformed second mode, but the trends of the eigenvalues that have been or will be determined at other values of the reduced frequency k may be used as a guide in making the selection that fits the trend.

In actual computations, one further cycle of iteration beginning with an assumed mode given by expression (A69) should be carried out to assess the extent to which the functions $w_{a2}^{(n-1)}$, $w_{a2}^{(n)}$, and $w_{a2}^{(n+1)}$ are free of all except the two components of the types appearing in equations (A60) and (A61). If the ratios of this cycle are not reasonably constant, the unwanted components still present have to be removed by carrying out another cycle of iteration and again applying equations (A64) and (A68).

The method just described is clearly applicable in the general cases $|C_n| = |C_{n+1}|$ or $|C_n| \approx |C_{n+1}|$.

Eigenvalues having equal moduli include the special case of identical eigenvalues. As a basis for discussion let it be assumed that

$$|C_1| > |C_2| = |C_3| > |C_4| > \ldots \tag{A70}$$

and that

$$C_2 = C_3 = C_{23} \tag{A71}$$

The significance of the occurrence of these two identical eigenvalues is that the wing system may oscillate with the same frequency and artificial damping in any of an infinite number of modes, any two of which are linearly independent of each other and of the first, fourth, and higher modes. This infinite number of possible modes (all corresponding to C_{23}) are the infinitely many linear combinations of two basic linearly independent modes that are necessary and sufficient in combination with the first, fourth, and higher modes to describe an arbitrary displacement of the wing system. Clearly, only two linearly independent modes corresponding to the double eigenvalue C_{23} are required for analytical purposes. These two are designated w_2 and w_3 as before

but with the reservation that w_2 and w_3 must be derivable as two differing linear combinations of a single basic pair of linearly independent modes that also correspond to C_{23}.

Equations (A20) and (A21) are replaced in the present case by

$$\lim_{n\to\infty} w_{a2}^{(n+1)} = \lim_{n\to\infty} C_{23}^{\,n}\left[b_2\left(w_2 - w_1\right) + b_3\left(w_3 - w_1\right)\right] \tag{A72}$$

and

$$\lim_{n\to\infty} \frac{w_{a2}^{(n+1)}}{w_{a2}^{(n)}} = C_{23} \tag{A73}$$

Equation (A27) is replaced by

$$\lim_{n\to\infty} w_{a2}^{(n+1)} + \frac{\lim_{n\to\infty} w_{b1}^{(n)}}{\frac{C_1}{C_{23}} - 1} = \lim_{n\to\infty} C_{23}^{\,n}\left(b_2 w_2 + b_3 w_3\right) \tag{A74}$$

The transformed second mode (equation (A72)) is in this case a linear combination of the first three eigenfunctions, and the so-called true second mode is actually a linear combination of the second and third eigenfunctions.

If the iterative transformation procedure is now applied in the regular way to determine the transformed third mode, the third eigenvalue, and the true third mode, the results will be as follows: The transformed third mode will be, like the transformed second mode, a linear combination of the first three eigenfunctions but will be linearly independent of the transformed second mode. The so-called true third mode will be, like the so-called true second mode, a linear combination of the second and third eigenfunctions and will be linearly independent of the so-called true second mode. The results will also include a second determination of the double eigenvalue C_{23}. It may therefore be concluded that the iterative transformation procedure is valid and sufficient in all cases of eigenvalue multiplicity.

APPENDIX B

THE COMPLEX STIFFNESS FOR BEAMS WITH STRUCTURAL DAMPING

The familiar concept of a complex force $K(1 + ig)s$ in simple (one-degree-of-freedom) vibrating systems having structural damping may be easily extended to continuous vibrating systems such as beams and airplane wings. The quantity K is the elastic-spring constant, s is the displacement, Ks is the elastic-spring force, and Kgs is the structural-damping force.

For a beam in flexure, the stiffness of the fibers is given by the modulus of elasticity E, which is analogous to the quantity K for the spring. The elastic stress at any point of the cross section is given by ϵE where ϵ is the strain which is analogous to the displacement s. Then the complex stress at any point of the cross section of a beam with structural damping is $E(1 + ig)\epsilon$. The complex bending moment corresponding to this stress, obtained in the usual way by integration of the moment of the stresses over the section, is $EI(1 + ig)\frac{d^2y}{dx^2}$. This result leads to the concept of a complex stiffness $EI(1 + ig_y)$ for beams in flexural vibration with structural damping. Similarly, the complex stiffness of beams in torsional vibration with structural damping is $GJ(1 + ig_\phi)$. The subscripts y and ϕ indicate that the structural-damping coefficient g may have a different value for torsional vibrations than it has for flexural vibrations. Both g_y and g_ϕ may be functions of the spanwise position x.

APPENDIX C

FORMULAS FOR EQUIVALENT CONCENTRATIONS AND INCREMENTS OF TORQUE

The formulas used in the numerical examples for computing equivalent concentrated loads and curvatures are those that have been derived in references 7 and 8. For the concentration at an end station the formula is

$$\bar{p}_1 = \frac{\lambda}{24}\left(7p_1 + 6p_2 - p_3\right) \tag{C1}$$

At an intermediate station

$$\bar{p}_2 = \frac{\lambda}{12}\left(p_1 + 10p_2 + p_3\right) \tag{C2}$$

The significance of the quantities used in formulas (C1) and (C2) is shown in the following sketch:

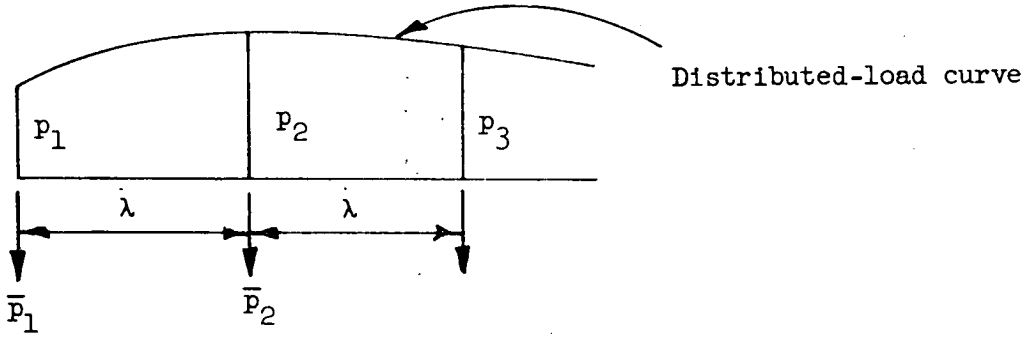

These formulas are based on the assumption that the distributed-load (or curvature) curve is a series of second-degree parabolic arcs. When applied to distributed flexural loads, the formulas give concentrations which produce the same bending moments in the wing at all the selected stations as the distributed load. The formulas may be correctly applied to distributed torsional loads only if GJ is constant over each bay. In this case the formulas give concentrations which produce the same torsional displacement at all the selected stations as the distributed load. For a station placed at a discontinuity in ordinate or slope,

formula (C1) must be applied to both the left and the right of the station and the results added.

The formulas for obtaining increments of area beneath a curve of distributed torques are derived in reference 8. These formulas are based as before on approximating second-degree parabolas. They are given here in a slightly different form which is better adapted to present uses. Thus

$$A_1 = \frac{\lambda}{6}\left(q_1 + 4q_2 + q_3\right) + \frac{\lambda}{4}\left(q_1 - q_3\right) \tag{C3}$$

$$A_2 = \frac{\lambda}{6}\left(q_1 + 4q_2 + q_3\right) - \frac{\lambda}{4}\left(q_1 - q_3\right) \tag{C4}$$

where the significance of A_1 and A_2 and of q_1, q_2, and q_3 is shown by the following sketch:

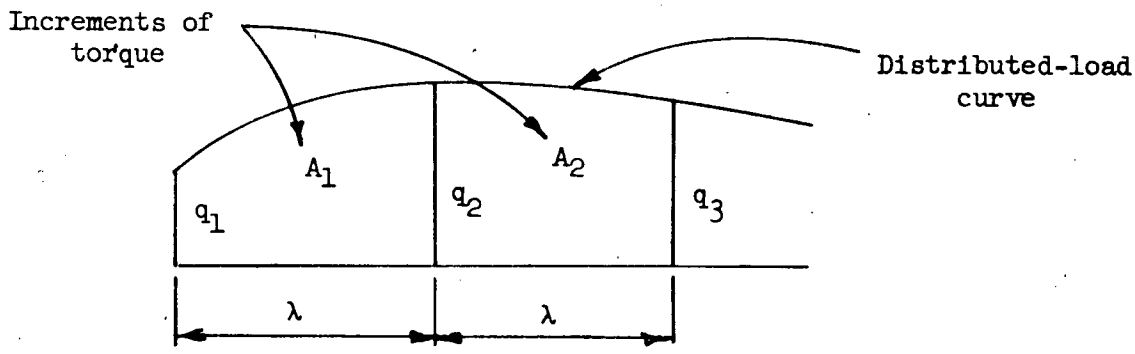

The ordinate at a discontinuity should not be used as the middle one of the three ordinates selected for use in formulas (C3) and (C4). The formulas are valid only where the three ordinates are connected by a continuous curve.

REFERENCES

1. Beskin, L., and Rosenberg, R. M.: Higher Modes of Vibration by a Method of Sweeping. Jour. Aero. Sci., vol. 13, no. 11, Nov. 1946, pp. 597-604.

2. Houbolt, John C., and Anderson, Roger A.: Calculation of Uncoupled Modes and Frequencies in Bending or Torsion of Nonuniform Beams. NACA TN 1522, 1948.

3. Wielandt, H.: Contributions to the Mathematical Treatment of Complex Eigenvalue Problems.

   II. The Iterative Method for Not Self-Adjoint Linear Eigenvalue Problems. Reps. and Translations No. 42, British M.A.P. Völkenrode, April 1, 1946. (Issued by Joint Intelligence Objectives Agency with File No. B.I.G.S. - 11.)

   III. The Iteration Procedure in the Flutter Calculation. Translation No. F-TS-904-RE, Air Materiel Command, U. S. Army Air Forces, Wright Field, Dayton, Ohio, (From Bericht B 44/J/21, Aerodynamische Versuchsanstalt Göttingen, Aug. 2, 1944) Oct. 1946.

4. Theodorsen, Theodore: General Theory of Aerodynamic Instability and the Mechanism of Flutter. NACA Rep. 496, 1935.

5. Runyan, Harry L., and Watkins, Charles E.: Flutter of a Uniform Wing with an Arbitrarily Placed Mass According to a Differential-Equation Analysis and a Comparison with Experiment. NACA Rep. 966, 1950.

6. Woolston, Donald S., and Runyan, Harry L.: Appraisal of Method of Flutter Analysis Based on Chosen Modes by Comparison with Experiment for Cases of Large Mass Coupling. NACA TN 1902, 1949.

7. Newmark, N. M.: Numerical Procedure for Computing Deflections, Moments, and Buckling Loads. Proc. A.S.C.E., vol. 68, no. 5, May 1942, pp. 691-718. (Also, Paper No. 2202, Trans. A.S.C.E., vol. 108, 1943, pp. 1161-1188.)

8. Benscoter, Stanley U., and Gossard, Myron L.: Matrix Methods for Calculating Cantilever-Beam Deflections. NACA TN 1827, 1949.

TABLE 1.- ITERATION TO OBTAIN FIRST COUPLED MODE FOR $k = \infty$. WING WITH CONCENTRATED MASS.

[Common factors for each column are given under the column headings.]

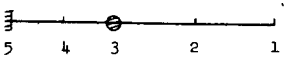

Station

Flexure: (a) First cycle.

Station	1	2	3	4	5	6	7	8	9	10	11	12	13	14	15	16	17	18	19
	$y_1^{(1)}$	P_{yy}	$P_{\phi\phi}$	p	$\bar{p}$	$\bar{p}$	$\bar{P}_{yy}$	$\bar{P}_{\phi\phi}$	$\bar{p}$	V	ΔM	M	α	$\bar{\alpha}$	$\bar{\alpha}$	β	Δy	$y_1^{(2)}$	$\frac{y_1^{(2)}}{y_1^{(1)}}$
	b	$\frac{b\gamma}{\mu}\omega^2$			$\frac{\lambda_1 b\gamma}{\mu}\omega^2$	$\frac{\lambda_o b\gamma}{\mu}\omega^2$					$\frac{\lambda_o^2 b\gamma}{\mu}\omega^2$		$\frac{\lambda_o^2 b\gamma}{EI\mu}\omega^2$	$\frac{\lambda_1\lambda_o^2 b\gamma}{EI\mu}\omega^2$	$\frac{\lambda_o^3 b\gamma}{EI\mu}\omega^2$		$\frac{\lambda_o^4 b\gamma}{EI\mu}\omega^2$		$\frac{\lambda_o^4\gamma}{EI\mu}\omega^2$
1	1.000	33.6	0	33.6	14.30	14.30			14.30	14.30	14.30	0	0					280.27	280.27
2	.568	19.10	0	19.10	19.26	19.26			19.26	33.56	33.56	14.30	14.30	15.90	15.90	120.90	120.90	159.37	280
3	.194	6.52	0	6.52	5.27 2.36	5.27 1.29	17.95	0	24.51	58.07	31.82	47.86	47.86	17.53 29.20	17.53 16.01	105.00	105.00	54.37	280
4	.054	1.82	0	1.82	2.06	1.13			1.13	59.20	32.45	79.68	79.68	79.75	43.70	71.46	39.15	15.22	282
5	0	0	0	0								112.13	112.13	50.60	27.76	27.76	15.22	0	

(b) Second cycle.

1	2	3
$y_1^{(2)}$	$y_1^{(3)}$	$\frac{y_1^{(3)}}{y_1^{(2)}}$
b	$\frac{\lambda_o^4 b\gamma}{EI\mu}\omega^2$	$\frac{\lambda_o^4\gamma}{EI\mu}\omega^2$
1.000	281.65	281.65
.569	160.24	282
.194	54.73	282
.054	15.33	284
0	0	

(c) Third cycle.

1	2	3	4
$y_1^{(3)}$	$y_1^{(4)}$	$\frac{y_1^{(4)}}{y_1^{(3)}}$	$\frac{\sum y_1^{(4)}}{\sum y_1^{(3)}}$
b	$\frac{\lambda_o^4 b\gamma}{EI\mu}\omega^2$	$\frac{\lambda_o^4\gamma}{EI\mu}\omega^2$	
1.000	281.90	281.90	
.570	160.36	282	
.194	54.75	282	282
.055	15.33	279	
0	0		

Torsion (with GJ constant over each bay): (a) First cycle.

Station	1	2	3	4	5	6	7	8	9	10	11	12	13	14	15
	$\phi_1^{(1)}$	Q_{yy}	$Q_{\phi\phi}$	q	$\bar{q}$	$\bar{q}$	$\bar{Q}_{yy}$	$\bar{Q}_{\phi\phi}$	$\bar{q}$	T	θ	$\Delta\phi$	$\phi_1^{(2)}$	$\phi_1^{(2)}$	$\frac{\phi_1^{(2)}}{\phi_1^{(1)}}$
		$\frac{b^2\gamma}{\mu}\omega^2$			$\frac{\lambda_1 b^2\gamma}{\mu}\omega^2$	$\frac{\lambda_o b^2\gamma}{\mu}\omega^2$					$\frac{\lambda_o b^2\gamma}{GJ\mu}\omega^2$	$\frac{\lambda_o^2 b^2\gamma}{GJ\mu}\omega^2$		$\frac{\lambda_o^4\gamma}{EI\mu}\omega^2$	
1	0	1.397	0	1.397	0.594	0.594			0.59					-12.28	-1.662	--
2	0	.794	0	.794	.800	.800			.80	0.59	0.59	0.59		-12.87	-1.742	--
3	0	.271	0	.271	.219 .098	.219 .054	-14.68	0	-14.41	1.39	1.39	1.39		-14.26	-1.930	--
4	0	.076	0	.076	.086	.047			.05	-13.02	-13.02	-7.15		-7.11	-.963	--
5	0	0	0	0						-12.97	-12.97	-7.11		0	0	

(b) Second cycle.

1	2	3
$\phi_1^{(2)}$	$\phi_1^{(3)}$	$\frac{\phi_1^{(3)}}{\phi_1^{(2)}}$
	$\frac{\lambda_o^4\gamma}{EI\mu}\omega^2$	
-0.00594	-1.780	300
-.00622	-1.861	299
-.00689	-2.048	297
-.00344	-1.022	297
0	0	

(c) Third cycle.

1	2	3	4
$\phi_1^{(3)}$	$\phi_1^{(4)}$	$\frac{\phi_1^{(4)}}{\phi_1^{(3)}}$	$\frac{\sum\phi_1^{(4)}}{\sum\phi_1^{(3)}}$
	$\frac{\lambda_o^4\gamma}{EI\mu}\omega^2$		
-0.00633	-1.786	282	
-.00662	-1.866	282	
-.00729	-2.056	282	282
-.00364	-1.026	282	
0	0	.	

$$\frac{1}{2}\left(\frac{\sum y_1^{(4)}}{\sum y_1^{(3)}} + \frac{\sum \phi_1^{(4)}}{\sum \phi_1^{(3)}}\right) = 282\,\frac{\lambda_o^4\gamma}{EI\mu}\omega^2$$

$$\omega_1 = \sqrt{\frac{EI\mu}{\lambda_o^4\gamma}\,282} = \sqrt{\frac{423{,}000}{282}}$$

= 38.7 radians per second

TABLE 1.- ITERATION TO OBTAIN FIRST COUPLED MODE FOR $k = \infty$. WING WITH CONCENTRATED MASS - Concluded

Torsion (with GJ variable): (a) First cycle.

Station	1	2	3	4	5	6	7	8	9	10	11	12	13	14	15	16	17
	$\phi_1^{(1)}$	Q_{yy}	$Q_{\phi\phi}$	q	ΔT	ΔT	T	$\overline{Q}_{yy}$	$\overline{Q}_{\phi\phi}$	T	T	θ	$\Delta\phi$	$\Delta\phi$	$\phi_1^{(2)}$	$\phi_1^{(2)}$	$\frac{\phi_1^{(2)}}{\phi_1^{(1)}}$
		$\frac{b^2\gamma}{\mu}\omega^2$			$\frac{\lambda_1 b^2\gamma}{\mu}\omega^2$		$\frac{\lambda_o b^2\gamma}{\mu}\omega^2$					$\frac{\lambda_o b^2\gamma}{GJ\mu}\omega^2$	$\frac{\lambda_1\lambda_o b^2\gamma}{GJ\mu}\omega^2$	$\frac{\lambda_o{}^2 b^2\gamma}{GJ\mu}\omega^2$		$\frac{\lambda_o{}^4\gamma}{EI\mu}\omega^2$	
1	0	1.397	0	1.397			0			0	0	0			-12.25	-1.660	--
					1.089	1.089							0.60	0.60			
2	0	.794	0	.794			1.089			0	1.09	1.09			-12.85	-1.741	--
					.525	.525							1.40	1.40			
3	0	.271	0	.271			1.614	-14.68	0	0 -14.68	1.61 -13.07	1.61 -13.07			-14.25	-1.929	--
					.164	.090							-13.02	-7.15			
4	0	.076	0	.076			1.704			-14.68	-12.98	-12.98			-7.10	-.962	--
					.028	.015							-12.96	-7.10			
5	0	0	0	0			1.719			-14.68	-12.96	-12.96			0	0	

NACA

TABLE 2.- ITERATION TO OBTAIN TRANSFORMED SECOND MODE FOR $k = \infty$. WING WITH CONCENTRATED MASS.

[Common factors for each column are given under the column headings.]

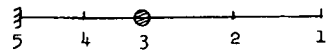

Station

Flexure: (a) First cycle. (b) Second cycle. (c) Third cycle.

Station	1	2	3	4	5	1	2	3	4	5	1	2	3	4	5	6
	$y^{(1)}_{a2}$	$y^{(1)}_{b}$	$y^{(1)}_{b1}$	$y^{(2)}_{a2}$	$\frac{y^{(2)}_{a2}}{y^{(1)}_{a2}}$	$y^{(2)}_{a2}$	$y^{(2)}_{b}$	$y^{(2)}_{b1}$	$y^{(3)}_{a2}$	$\frac{y^{(3)}_{a2}}{y^{(2)}_{a2}}$	$y^{(3)}_{a2}$	$y^{(3)}_{b}$	$y^{(3)}_{b1}$	$y^{(4)}_{a2}$	$\frac{y^{(4)}_{a2}}{y^{(3)}_{a2}}$	$\frac{\sum y^{(4)}_{a2}}{\sum y^{(3)}_{a2}}$
	b	$\frac{\lambda_o^4 b\gamma}{EI\mu}\omega^2$			$\frac{\lambda_o^4 \gamma}{EI\mu}\omega^2$	b	$\frac{\lambda_o^4 b\gamma}{EI\mu}\omega^2$			$\frac{\lambda_o^4 \gamma}{EI\mu}\omega^2$	b	$\frac{\lambda_o^4 b\gamma}{EI\mu}\omega^2$			$\frac{\lambda_o^4 \gamma}{EI\mu}\omega^2$	
1(A)	0	-174.1	174.1	0		0	-411.0	411.0	0		0	-465.8	465.8	0		
2	-.281	-107.7	99.2	-8.5	30.2	-.692	-252.5	234.2	-18.3	26.4	-.820	-285.4	265.4	-20.0	24.4	
3	-.252	-43.1	33.8	-9.3	36.9	-.757	-99.7	80.0	-19.7	26.0	-.882	-112.0	90.6	-21.4	24.2	24.3
4	-.094	-13.1	9.48	-3.6	38.3	-.293	-30.2	22.4	-7.8	26.6	-.349	-33.8	25.4	-8.4	24.1	
5	0	0	0	0		0	0	0	0		0	0	0	0		

Torsion: (a) First cycle. (b) Second cycle. (c) Third cycle.

Station	1	2	3	4	5	1	2	3	4	5	1	2	3	4	5	6
	$\phi^{(1)}_{a2}$	$\phi^{(1)}_{b}$	$\phi^{(1)}_{b1}$	$\phi^{(2)}_{a2}$	$\frac{\phi^{(2)}_{a2}}{\phi^{(1)}_{a2}}$	$\phi^{(2)}_{a2}$	$\phi^{(2)}_{b}$	$\phi^{(2)}_{b1}$	$\phi^{(3)}_{a2}$	$\frac{\phi^{(3)}_{a2}}{\phi^{(2)}_{a2}}$	$\phi^{(3)}_{a2}$	$\phi^{(3)}_{b}$	$\phi^{(3)}_{b1}$	$\phi^{(4)}_{a2}$	$\frac{\phi^{(4)}_{a2}}{\phi^{(3)}_{a2}}$	$\frac{\sum \phi^{(4)}_{a2}}{\sum \phi^{(3)}_{a2}}$
		$\frac{\lambda_o^4 \gamma}{EI\mu}\omega^2$					$\frac{\lambda_o^4 \gamma}{EI\mu}\omega^2$					$\frac{\lambda_o^4 \gamma}{EI\mu}\omega^2$				
1	1.000	13.38	-1.10	12.28	12.28	1.000	24.94	-2.60	22.34	22.34	1.000	26.22	-2.95	23.27	23.27	
2	.901	13.38	-1.15	12.23	13.58	.997	24.95	-2.72	22.23	22.3	.995	26.24	-3.08	23.16	23.3	
3	.624	13.40	-1.28	12.12	19.44	.988	25.05	-3.00	22.05	22.3	.988	26.40	-3.40	23.00	23.3	23.3
4	.322	6.70	-.63	6.07	18.85	.495	12.51	-1.50	11.01	22.2	.493	13.20	-1.70	11.50	23.3	
5	0	0	0	0		0	0	0	0		0	0	0	0		

$$\frac{1}{2}\left(\frac{\sum y^{(4)}_{a2}}{\sum y^{(3)}_{a2}} + \frac{\sum \phi^{(4)}_{a2}}{\sum \phi^{(3)}_{a2}}\right) = 23.8\,\frac{\lambda_o^4 \gamma}{EI\mu}\omega^2; \quad \omega_2 = 133.3 \text{ radians per second}$$

NACA

TABLE 3.- ITERATION TO OBTAIN TRANSFORMED THIRD MODE FOR $k = \infty$. WING WITH CONCENTRATED MASS.

[Common factors for each column are given under each column heading.]

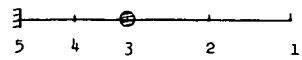

Station

Flexure: (a) First cycle.

Station	1	2	3	4	5	6
	$y_{a3}^{(1)}$	$y_b^{(1)}$	$y_{bl}^{(1)}$	$y_{ba2}^{(1)}$	$y_{a3}^{(2)}$	$\frac{y_{a3}^{(2)}}{y_{a3}^{(1)}}$
	b	$\frac{\lambda_o^4 b\gamma}{EI\mu}\omega^2$				$\frac{\lambda_o^4 \gamma}{EI\mu}\omega^2$
1(A)	0	448.1	-440.1	0	0	
2	.952	271.5	-254.8	-11.1	5.6	5.9
3	1.000	104.0	-87.0	-11.9	5.1	5.1
4	.390	31.0	-24.4	-4.7	1.9	4.9
5	0	0	0	0	0	

(b) Second cycle.

1	2	3	4	5	6
$y_{a3}^{(2)}$	$y_b^{(2)}$	$y_{bl}^{(2)}$	$y_{ba2}^{(2)}$	$y_{a3}^{(3)}$	$\frac{y_{a3}^{(3)}}{y_{a3}^{(2)}}$
b	$\frac{\lambda_o^4 b\gamma}{EI\mu}\omega^2$				$\frac{\lambda_o^4 \gamma}{EI\mu}\omega^2$
0	405.5	-405.5	0	0	
1.000	243.7	-230.6	-5.9	7.2	7.2
.911	91.6	-78.8	-6.3	6.5	7.2
.339	27.0	-22.1	-2.5	2.4	7.1
0	0	0	0	0	

(c) Third cycle.

1	2	3	4	5	6	7
$y_{a3}^{(3)}$	$y_b^{(3)}$	$y_{bl}^{(3)}$	$y_{ba2}^{(3)}$	$y_{a3}^{(4)}$	$\frac{y_{a3}^{(4)}}{y_{a3}^{(3)}}$	$\frac{\sum y_{a3}^{(4)}}{\sum y_{a3}^{(3)}}$
b	$\frac{\lambda_o^4 b\gamma}{EI\mu}\omega^2$				$\frac{\lambda_o^4 \gamma}{EI\mu}\omega^2$	
0	404.0	-404.0	0	0		
1.000	242.8	-230.0	-5.9	6.9	6.9	
.903	91.3	-78.5	-6.3	6.5	7.2	7.07
.333	26.9	-22.0	-2.5	2.4	7.1	
0	0	0	0	0		

Torsion: (a) First cycle.

Station	1	2	3	4	5	6
	$\phi_{a3}^{(1)}$	$\phi_b^{(1)}$	$\phi_{bl}^{(1)}$	$\phi_{ba2}^{(1)}$	$\phi_{a3}^{(2)}$	$\frac{\phi_{a3}^{(2)}}{\phi_{a3}^{(1)}}$
		$\frac{\lambda_o^4 \gamma}{EI\mu}\omega^2$				
1(B)	0	-15.79	2.84	12.95	0	
2	-.083	-15.81	2.96	12.88	.13	-1.6
3	-.304	-16.03	3.26	12.80	.03	-.1
4	-.150	-8.00	1.63	6.40	.03	-.2
5	0	0	0	0	0	

(b) Second cycle.

1	2	3	4	5	6
$\phi_{a3}^{(2)}$	$\phi_b^{(2)}$	$\phi_{bl}^{(2)}$	$\phi_{ba2}^{(2)}$	$\phi_{a3}^{(3)}$	$\frac{\phi_{a3}^{(3)}}{\phi_{a3}^{(2)}}$
	$\frac{\lambda_o^4 \gamma}{EI\mu}\omega^2$				
0	-9.46	2.57	6.89	0	
.0232	-9.50	2.68	6.85	.03	1.3
.0054	-9.72	2.96	6.80	.04	7
.0054	-4.85	1.48	3.40	.03	6
0	0	0	0	0	

(c) Third cycle.

1	2	3	4	5	6	7
$\phi_{a3}^{(3)}$	$\phi_b^{(3)}$	$\phi_{bl}^{(3)}$	$\phi_{ba2}^{(3)}$	$\phi_{a3}^{(4)}$	$\frac{\phi_{a3}^{(4)}}{\phi_{a3}^{(3)}}$	$\frac{\sum \phi_{a3}^{(4)}}{\sum \phi_{a3}^{(3)}}$
	$\frac{\lambda_o^4 \gamma}{EI\mu}\omega^2$					
0	-9.46	2.56	6.90	0		
.0042	-9.50	2.68	6.86	.04	10.0	
.0056	-9.72	2.94	6.81	.03	5	7.15
.0042	-4.85	1.47	3.41	.03	7	
0	0	0	0	0		

NACA

$$\frac{1}{2}\left(\frac{\sum y_{a3}^{(4)}}{\sum y_{a3}^{(3)}} + \frac{\sum \phi_{a3}^{(4)}}{\sum \phi_{a3}^{(3)}}\right) = 7.11 \frac{\lambda_o^4 \gamma}{EI\mu}\omega^2; \quad \omega_3 = 244 \text{ radians per second}$$

TABLE 4.- AERODYNAMIC-INERTIA FORCE COEFFICIENTS FOR VARIOUS VALUES OF k FOR EXAMPLE WING

[Common factors for each column are given under the column headings.]

Flexure

k	P_{Ry}	$P_{R\phi}$	P_{Iy}	$P_{I\phi}$	$\bar{P}_{Ry}$	$\bar{P}_{R\phi}$
	$\frac{\gamma}{\mu}\omega^2$	$\frac{b\gamma}{\mu}\omega^2$	$\frac{\gamma}{\mu}\omega^2$	$\frac{b\gamma}{\mu}\omega^2$	$\frac{\lambda_o\gamma}{\mu}\omega^2$	$\frac{\lambda_o b\gamma}{\mu}\omega^2$
0.036	27.5	-1444	51.9	-108.3	92.5	-75.6
.12	30.6	-112.5	13.44	-8.27	92.5	-75.6
.1443	31.0	-75.2	10.82	-4.14	92.5	-75.6
.1590	31.2	-60.7	9.61	-2.53	92.5	-75.6
.24	32.0	-23.8	5.82	1.35	92.5	-75.6
.50	33.0	-3.76	2.39	2.29	92.5	-75.6
∞	33.6	1.397	0	0	92.5	-75.6

Torsion

k	Q_{Ry}	$Q_{R\phi}$	Q_{Iy}	$Q_{I\phi}$	$\bar{Q}_{Ry}$	$\bar{Q}_{R\phi}$
	$\frac{b\gamma}{\mu}\omega^2$	$\frac{b^2\gamma}{\mu}\omega^2$	$\frac{b\gamma}{\mu}\omega^2$	$\frac{b^2\gamma}{\mu}\omega^2$	$\frac{\lambda_o b\gamma}{\mu}\omega^2$	$\frac{\lambda_o b^2\gamma}{\mu}\omega^2$
0.036	3.67	549	-19.40	68.3	-75.6	114.7
.12	2.52	51.4	-5.03	11.42	-75.6	114.7
.1443	2.36	37.5	-4.05	8.48	-75.6	114.7
.1590	2.28	32.0	-3.60	7.24	-75.6	114.7
.24	1.98	18.24	-2.18	3.67	-75.6	114.7
.50	1.623	10.74	-.895	1.143	-75.6	114.7
∞	1.397	.1409	0	0	-75.6	114.7

TABLE 5.- ITERATION TO OBTAIN FIRST MODE FOR k = 0.1443. WING WITH CONCENTRATED MASS.

[Common factors for each column are given under the column headings.]

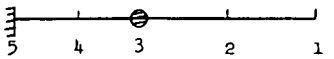

Station

Flexure: (a) First cycle.

Station	1	2	3	4	5	6	7	8	9	10	11	12	13	14	15	16	17	18	19	20	21
	$y_{1R}^{(1)}$	$y_{1I}^{(1)}$	$P_{Ry}y_R$	$P_{R\phi}\phi_R$	$P_{Iy}y_I$	$P_{I\phi}\phi_I$	P_R	$\bar{P}_R$	$\bar{P}_R$	$\bar{P}_{Ry}y_R$	$\bar{P}_{R\phi}\phi_R$	$\bar{P}_R$	V_R	ΔM_R	M_R	α	$\bar{\alpha}$	$\bar{\alpha}$	β	Δy	$y_{1R}^{(2)}$
	b		$\frac{b\gamma}{\mu}\omega^2$					$\frac{\lambda_1 b\gamma}{\mu}\omega^2$	$\frac{\lambda_0 b\gamma}{\mu}\omega^2$					$\frac{\lambda_0^2 b\gamma}{\mu}\omega^2$		$\frac{\lambda_0^2 b\gamma}{EI\mu}\frac{1}{C}$	$\frac{\lambda_1\lambda_0^2 b\gamma}{EI\mu}\frac{1}{C}$	$\frac{\lambda_0^3 b\gamma}{EI\mu}\frac{1}{C}$		$\frac{\lambda_0^4 b\gamma}{EI\mu}\frac{1}{C}$	
1	1.000	0	31.0	0	0	0	31.0	12.34	12.34			12.34			0	0					218.6
													12.34	12.34					95.3	95.3	
2	.444	0	13.77	0	0	0	13.77	14.35	14.35			14.35			12.34	12.34	13.5	13.5			123.3
													26.69	26.69					81.8	81.8	
3	.111	0	3.44	0	0	0	3.44	{3.16 1.22	{3.16 .67	10.27	0	14.10			39.03	39.03	{14.5 23.2	{14.5 12.7			41.5
													40.79	22.38					54.6	30.0	
4	.028	0	.868	0	0	0	.868	1.01	.55			.55			61.41	61.41	61.5	33.7			11.5
													41.34	22.62					20.9	11.5	
5	0	0	0	0	0	0	0								84.03	84.03	38.2	20.9			0

Torsion: (a) First cycle.

Station	1	2	3	4	5	6	7	8	9	10	11	12	13	14	15	16	17
	$\phi_{1R}^{(1)}$	$\phi_{1I}^{(1)}$	$Q_{Ry}y_R$	$Q_{R\phi}\phi_R$	$Q_{Iy}y_I$	$Q_{I\phi}\phi_I$	q_R	$\bar{q}_R$	$\bar{q}_R$	$\bar{Q}_{Ry}y_R$	$\bar{Q}_{R\phi}\phi_R$	$\bar{q}_R$	T_R	θ	$\Delta\phi$	$\phi_{1R}^{(2)}$	$\phi_{1R}^{(2)}$
			$\frac{b^2\gamma}{\mu}\omega^2$					$\frac{\lambda_1 b^2\gamma}{\mu}\omega^2$	$\frac{\lambda_0 b^2\gamma}{\mu}\omega^2$					$\frac{\lambda_0 b^2\gamma}{GJ\mu}\frac{1}{C}$	$\frac{\lambda_0^2 b^2\gamma}{GJ\mu}\frac{1}{C}$		$\frac{\lambda_0^4\gamma}{EI\mu}\frac{1}{C}$
1	0	0	2.36	0	0	0	2.36	0.939	0.939			0.939				-3.77	-0.510
													0.94	0.94	0.94		
2	0	0	1.048	0	0	0	1.048	1.092	1.092			1.092				-4.71	-.638
													2.03	2.03	2.03		
3	0	0	.262	0	0	0	.262	{.240 .093	{.240 .051	-8.50	0	-8.21				-6.74	-.912
													-6.18	-6.18	-3.38		
4	0	0	.0660	0	0	0	.0660	.077	.042			.042				-3.36	-.455
													-6.14	-6.14	-3.36		
5	0	0	0	0	0	0	0									0	0

TABLE 5.- ITERATION TO OBTAIN FIRST MODE FOR k = 0.1443. WING WITH CONCENTRATED MASS - Continued

Flexure: (a) First cycle - Concluded

Station	22	23	24	25	26	27	28	29	30	31	32	33	34	35	36	37	38	39	40	41
	P_{Ry_I}	$P_{R\phi_I}$	$-P_{Iy_R}$	$-P_{I\phi_R}$	P_I	$\bar{P}_I$	$\bar{p}_I$	$\bar{P}_{Ry_I}$	$\bar{P}_{R\phi_I}$	$\bar{p}_I$	V_I	ΔM_I	M_I	α	$\bar{\alpha}$	$\bar{\alpha}$	β	Δy	$y_{1I}^{(2)}$	$\frac{y_{1R}^{(2)} + iy_{1I}^{(2)}}{y_{1R}^{(1)} + iy_{1I}^{(1)}}$
	$\frac{b\gamma}{\mu}\omega^2$					$\frac{\lambda_1 b\gamma}{\mu}\omega^2$	$\frac{\lambda_o b\gamma}{\mu}\omega^2$					$\frac{\lambda_o^2 b\gamma}{\mu}\omega^2$		$\frac{\lambda_o^2 b\gamma}{EI\mu}\frac{1}{C}$	$\frac{\lambda_1\lambda_o^2 b\gamma}{EI\mu}\frac{1}{C}$	$\frac{\lambda_o^3 b\gamma}{EI\mu}\frac{1}{C}$		$\frac{\lambda_o^4 b\gamma}{EI\mu}\frac{1}{C}$		$\frac{\lambda_o^4\gamma}{EI\mu}\frac{1}{C}$
1	0	0	-10.82	0	-10.82	-4.31	-4.31			-4.31			0	0					-70.38	218.6 - 70.381
											-4.31	-4.31					-31.12	-31.12		
2	0	0	-4.80	0	-4.80	-5.00	-5.00			-5.00			-4.31	-4.31	-4.73	-4.73			-39.26	----------
											-9.31	-9.31					-26.39	-26.39		
3	0	0	-1.201	0	-1.201	{-1.099 {-.426	{-1.099 {-.234	0	0	-1.333			-13.62	-13.62	{-5.05 {-7.77	{-5.05 {-4.26			-12.87	374 - 116.01
											-10.64	-5.84					-17.08	-9.35		
4	0	0	-.303	0	-.303	-.352	-.193			-.193			-19.46	-19.46	-19.46	-10.67			-3.52	----------
											-10.83	-5.95					-6.41	-3.52		
5	0	0	0	0	0								-25.41	-25.41	-11.70	-6.41			0	

Torsion: (a) First cycle - Concluded

Station	18	19	20	21	22	23	24	25	26	27	28	29	30	31	32	33
	Q_{Ry_I}	$Q_{R\phi_I}$	$-Q_{Iy_R}$	$-Q_{I\phi_R}$	q_I	$\bar{q}_I$	$\bar{q}_I$	$\bar{Q}_{Ry_I}$	$\bar{Q}_{R\phi_I}$	$\bar{q}_I$	T_I	θ	$\Delta\phi$	$\phi_{1I}^{(2)}$	$\phi_{1I}^{(2)}$	$\frac{\phi_{1R}^{(2)} + i\phi_{1I}^{(2)}}{\phi_{1R}^{(1)} + i\phi_{1I}^{(1)}}$
	$\frac{b^2\gamma}{\mu}\omega^2$					$\frac{\lambda_1 b^2\gamma}{\mu}\omega^2$	$\frac{\lambda_o b^2\gamma}{\mu}\omega^2$					$\frac{\lambda_o b^2\gamma}{GJ\mu}\frac{1}{C}$	$\frac{\lambda_o^2 b^2\gamma}{GJ\mu}\frac{1}{C}$			$\frac{\lambda_o^4\gamma}{EI\mu}\frac{1}{C}$
1	0	0	4.05	0	4.05	1.612	1.612			1.612				9.51	1.288	------
											1.612	1.612	1.61			
2	0	0	1.798	0	1.798	1.874	1.874			1.874				7.90	1.070	------
											3.486	3.486	3.49			
3	0	0	.450	0	.450	{.412 {.160	{.412 {.088	0	0	.500				4.41	.597	------
											3.986	3.986	2.18			
4	0	0	.1143	0	.1143	.133	.073			.073				2.23	.302	------
											4.059	4.059	2.23			
5	0	0	0	0	0									0	0	

TABLE 5.- ITERATION TO OBTAIN FIRST MODE FOR $k = 0.1443$. WING WITH CONCENTRATED MASS - Concluded

Flexure: (b) Second cycle.

Station	1	2	3	4	5
	$y_{1R}^{(2)}$	$y_{1I}^{(2)}$	$y_{1R}^{(3)}$	$y_{1I}^{(3)}$	$\frac{y_{1R}^{(3)} + iy_{1I}^{(3)}}{y_{1R}^{(2)} + iy_{1I}^{(2)}}$
	b		$\frac{\lambda_o^4 b\gamma}{EI\mu}\frac{1}{C}$		$\frac{\lambda_o^4 \gamma}{EI\mu}\frac{1}{C}$
1	1.000	0	263.0	-83.22	263.0 - 83.221
2	.563	.0015	149.7	-46.67	------
3	.189	.0021	51.2	-15.42	270 - 84.91
4	.052	.0007	14.4	-4.22	------
5	0	0	0	0	

(c) Third cycle.

1	2	3	4	5
$y_{1R}^{(3)}$	$y_{1I}^{(3)}$	$y_{1R}^{(4)}$	$y_{1I}^{(4)}$	$\frac{y_{1R}^{(4)} + iy_{1I}^{(4)}}{y_{1R}^{(3)} + iy_{1I}^{(3)}}$
b		$\frac{\lambda_o^4 b\gamma}{EI\mu}\frac{1}{C}$		$\frac{\lambda_o^4 \gamma}{EI\mu}\frac{1}{C}$
1.000	0	267.5	-82.89	267.5 - 82.891
.569	.0020	152.3	-46.47	------
.194	.0028	52.1	-15.33	268 - 83.21
.054	.0012	14.6	-4.20	------
0	0	0	0	

(d) Fourth cycle.

1	2	3	4	5	6
$y_{1R}^{(4)}$	$y_{1I}^{(4)}$	$y_{1R}^{(5)}$	$y_{1I}^{(5)}$	$\frac{y_{1R}^{(5)} + iy_{1I}^{(5)}}{y_{1R}^{(4)} + iy_{1I}^{(4)}}$	$\frac{\sum\left(y_{1R}^{(5)} + iy_{1I}^{(5)}\right)}{\sum\left(y_{1R}^{(4)} + iy_{1I}^{(4)}\right)}$
b		$\frac{\lambda_o^4 b\gamma}{EI\mu}\frac{1}{C}$		$\frac{\lambda_o^4 \gamma}{EI\mu}\frac{1}{C}$	
1.000	0	268.6	-82.56	268.6 - 82.561	
.569	.0030	153.0	-46.29	------	
.194	.0027	52.4	-15.28	270 - 82.51	269 - 82.81
.054	.0011	14.7	-4.18	------	
0	0	0	0		

Torsion: (b) Second cycle.

Station	1	2	3	4	5
	$\phi_{1R}^{(2)}$	$\phi_{1I}^{(2)}$	$\phi_{1R}^{(3)}$	$\phi_{1I}^{(3)}$	$\frac{\phi_{1R}^{(3)} + i\phi_{1I}^{(3)}}{\phi_{1R}^{(2)} + i\phi_{1I}^{(2)}}$
			$\frac{\lambda_o^4 \gamma}{EI\mu}\frac{1}{C}$		
1	-0.00382	0.00466	-1.407	1.601	353 + 12.11
2	-.00407	.00358	-1.537	1.353	-----
3	-.00457	.00126	-1.829	.773	414 - 55.11
4	-.00228	.00064	-.912	.392	-----
5	0	0	0	0	

(c) Third cycle.

1	2	3	4	5
$\phi_{1R}^{(3)}$	$\phi_{1I}^{(3)}$	$\phi_{1R}^{(4)}$	$\phi_{1I}^{(4)}$	$\frac{\phi_{1R}^{(4)} + i\phi_{1I}^{(4)}}{\phi_{1R}^{(3)} + i\phi_{1I}^{(3)}}$
		$\frac{\lambda_o^4 \gamma}{EI\mu}\frac{1}{C}$		
-0.00660	0.00399	-1.570	1.594	282 - 71.51
-.00680	.00300	-1.690	1.350	-----
-.00716	.00068	-1.963	.764	282 - 79.81
-.00358	.00036	-.982	.387	-----
0	0	0	0	

(d) Fourth cycle.

1	2	3	4	5	6
$\phi_{1R}^{(4)}$	$\phi_{1I}^{(4)}$	$\phi_{1R}^{(5)}$	$\phi_{1I}^{(5)}$	$\frac{\phi_{1R}^{(5)} + i\phi_{1I}^{(5)}}{\phi_{1R}^{(4)} + i\phi_{1I}^{(4)}}$	$\frac{\sum\left(\phi_{1R}^{(5)} + i\phi_{1I}^{(5)}\right)}{\sum\left(\phi_{1R}^{(4)} + i\phi_{1I}^{(4)}\right)}$
		$\frac{\lambda_o^4 \gamma}{EI\mu}\frac{1}{C}$			
-0.00704	0.00379	-1.591	1.589	270 - 80.81	
-.00720	.00281	-1.711	1.340	-----	
-.00751	.00052	-1.977	.758	269 - 82.41	270 - 81.51
-.00376	.00028	-.988	.384	-----	
0	0	0	0		

NACA

$$\frac{1}{2}\left[\frac{\sum\left(y_{1R}^{(5)} + iy_{1I}^{(5)}\right)}{\sum\left(y_{1R}^{(4)} + iy_{1I}^{(4)}\right)} + \frac{\sum\left(\phi_{1R}^{(5)} + i\phi_{1I}^{(5)}\right)}{\sum\left(\phi_{1R}^{(4)} + i\phi_{1I}^{(4)}\right)}\right] = (269.5 - 82.21)\frac{\lambda_o^4 \gamma}{EI\mu}\frac{1}{C};\ \omega_1 = \sqrt{\frac{423{,}000}{269.5}} = 39.7 \text{ radians per second};\ g_{al} = \frac{-82.2}{269.5} = -0.305;\ v_1 = \frac{1}{3}\frac{39.7}{0.1443} = 91.6 \text{ feet per second}$$

TABLE 6.- ITERATION TO OBTAIN TRANSFORMED SECOND MODE FOR $k = 0.1443$. WING WITH CONCENTRATED MASS.

[Common factors for each column are given under the column headings.]

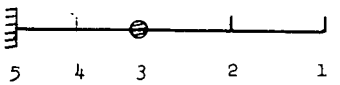

Flexure: (a) First cycle.

Station	1	2	3	4	5	6	7	8	9
	$y^{(1)}_{a2R}$	$y^{(1)}_{a2I}$	$y^{(1)}_{bR}$	$y^{(1)}_{bI}$	$y^{(1)}_{b1R}$	$y^{(1)}_{b1I}$	$y^{(2)}_{a2R}$	$y^{(2)}_{a2I}$	$\frac{y^{(2)}_{a2R} + iy^{(2)}_{a2I}}{y^{(1)}_{a2R} + iy^{(1)}_{a2I}}$
	b		$\frac{\lambda_o^4 b\gamma}{EI\mu}\frac{1}{C}$						$\frac{\lambda_o^4 \gamma}{EI\mu}\frac{1}{C}$
1(A)	0	0	-818.4	41.38	818.4	-41.38	0	0	
2	0	0	-468.8	23.48	464.5	21.8	-4.3	1.7	------
3	0	0	-161.4	7.90	158.8	-5.7	-2.6	2.2	------
4	0	0	-45.4	2.19	44.5	-1.31	-.9	.88	------
5	0	0	0	0	0	0	0	0	

(b) Second cycle.

1	2	3	4	5	6	7	8	9
$y^{(2)}_{a2R}$	$y^{(2)}_{a2I}$	$y^{(2)}_{bR}$	$y^{(2)}_{bI}$	$y^{(2)}_{b1R}$	$y^{(2)}_{b1I}$	$y^{(3)}_{a2R}$	$y^{(3)}_{a2I}$	$\frac{y^{(3)}_{a2R} + iy^{(3)}_{a2I}}{y^{(2)}_{a2R} + iy^{(2)}_{a2I}}$
b		$\frac{\lambda_o^4 b\gamma}{EI\mu}\frac{1}{C}$						$\frac{\lambda_o^4 \gamma}{EI\mu}\frac{1}{C}$
0	0	-888.5	104.65	888.5	-104.65	0	0	
-.188	.064	-510.8	61.60	504.5	-57.1	-6.3	4.5	37 - 11.21
-.117	.090	-177.0	22.28	172.5	-17.7	-4.5	4.6	43 - 6.11
-.041	.036	-50.0	6.45	48.4	-4.64	-1.6	1.81	------
0	0	0	0	0	0	0	0	

Torsion: (a) First cycle.

Station	1	2	3	4	5	6	7	8	9
	$\phi^{(1)}_{a2R}$	$\phi^{(1)}_{a2I}$	$\phi^{(1)}_{bR}$	$\phi^{(1)}_{bI}$	$\phi^{(1)}_{b1R}$	$\phi^{(1)}_{b1I}$	$\phi^{(2)}_{a2R}$	$\phi^{(2)}_{a2I}$	$\frac{\phi^{(2)}_{a2R} + i\phi^{(2)}_{a2I}}{\phi^{(1)}_{a2R} + i\phi^{(1)}_{a2I}}$
			$\frac{\lambda_o^4 \gamma}{EI\mu}\frac{1}{C}$						
1	1.000	0	28.76	-4.45	-5.62	3.35	23.14	-1.10	23.14 - 1.10i
2	.875	0	26.25	-3.89	-5.79	2.56	20.46	-1.33	------
3	.529	0	19.42	-2.35	-6.12	.73	13.30	-1.62	25.2 - 3.06i
4	.274	0	9.92	-1.222	-3.06	.379	6.86	-.84	------
5	0	0	0	0	0	0	0	0	

(b) Second cycle.

1	2	3	4	5	6	7	8	9
$\phi^{(2)}_{a2R}$	$\phi^{(2)}_{a2I}$	$\phi^{(2)}_{bR}$	$\phi^{(2)}_{bI}$	$\phi^{(2)}_{b1R}$	$\phi^{(2)}_{b1I}$	$\phi^{(3)}_{a2R}$	$\phi^{(3)}_{a2I}$	$\frac{\phi^{(3)}_{a2R} + i\phi^{(3)}_{a2I}}{\phi^{(2)}_{a2R} + i\phi^{(2)}_{a2I}}$
		$\frac{\lambda_o^4 \gamma}{EI\mu}\frac{1}{C}$						
1.000	0	30.80	-6.92	-5.88	4.05	24.92	-2.87	24.92 - 2.87i
.886	-.0153	28.36	-6.33	-6.12	3.21	22.24	-3.12	------
.577	-.0426	21.60	-4.59	-6.61	1.24	14.99	-3.35	26.2 - 3.86i
.298	-.0221	11.01	-2.36	-3.30	.63	7.71	-1.73	------
0	0	0	0	0	0	0	0	

NACA

TABLE 6.- ITERATION TO OBTAIN TRANSFORMED SECOND MODE FOR $k = 0.1443$. WING WITH CONCENTRATED MASS - Concluded

Flexure: (c) Third cycle.

Station	1	2	3	4	5	6	7	8	9
	$y^{(3)}_{a2R}$	$y^{(3)}_{a2I}$	$y^{(3)}_{bR}$	$y^{(3)}_{bI}$	$y^{(3)}_{blR}$	$y^{(3)}_{blI}$	$y^{(4)}_{a2R}$	$y^{(4)}_{a2I}$	$\frac{y^{(4)}_{a2R} + iy^{(4)}_{a2I}}{y^{(3)}_{a2R} + iy^{(3)}_{a2I}}$
	b		$\frac{\lambda_o^4 b\gamma}{EI\mu}\frac{1}{C}$						$\frac{\lambda_o^4 \gamma}{EI\mu}\frac{1}{C}$
1(A)	0	0	-931.9	156.25	931.9	-156.25	0	0	
2	-.271	.149	-537.2	92.18	530.5	-86.3	-6.7	5.9	28 - 6.31
3	-.199	.161	-187.2	32.98	181.2	-27.7	-6.0	5.3	31 - 1.41
4	-.071	.065	-53.0	9.60	50.8	-7.41	-2.2	2.19	32 - 1.41
5	0	0	0	0	0	0	0	0	

(d) Fourth cycle.

Station	1	2	3	4	5	6	7	8	9	10
	$y^{(4)}_{a2R}$	$y^{(4)}_{a2I}$	$y^{(4)}_{bR}$	$y^{(4)}_{bI}$	$y^{(4)}_{blR}$	$y^{(4)}_{blI}$	$y^{(5)}_{a2R}$	$y^{(5)}_{a2I}$	$\frac{y^{(5)}_{a2R} + iy^{(5)}_{a2I}}{y^{(4)}_{a2R} + iy^{(4)}_{a2I}}$	$\frac{\sum\left(y^{(5)}_{a2R} + iy^{(5)}_{a2I}\right)}{\sum\left(y^{(4)}_{a2R} + iy^{(4)}_{a2I}\right)}$
	b		$\frac{\lambda_o^4 b\gamma}{EI\mu}\frac{1}{C}$						$\frac{\lambda_o^4 \gamma}{EI\mu}\frac{1}{C}$	
1	0	0	-941.0	165.58	941.0	-165.58	0	0		
2	-.281	.184	-543.3	98.06	534.9	-91.8	-8.4	6.3	31 - 2.01	
3	-.252	.165	-190.0	35.82	183.1	-29.50	-6.9	6.32	31 - 5.01	31 - 3.41i
4	-.094	.069	-54.0	10.42	51.3	-7.93	-2.7	2.49	31 - 3.51	
5	0	0	0	0	0	0	0	0		

Torsion: (c) Third cycle.

Station	1	2	3	4	5	6	7	8	9
	$\phi^{(3)}_{a2R}$	$\phi^{(3)}_{a2I}$	$\phi^{(3)}_{bR}$	$\phi^{(3)}_{bI}$	$\phi^{(3)}_{blR}$	$\phi^{(3)}_{blI}$	$\phi^{(4)}_{a2R}$	$\phi^{(4)}_{a2I}$	$\frac{\phi^{(4)}_{a2R} + i\phi^{(4)}_{a2I}}{\phi^{(3)}_{a2R} + i\phi^{(3)}_{a2I}}$
			$\frac{\lambda_o^4 \gamma}{EI\mu}\frac{1}{C}$						
1	1.000	0	32.38	-8.42	-6.00	4.60	26.38	-3.82	26.38 - 3.821
2	.904	-.0221	29.90	-7.81	-6.29	3.71	23.61	-4.10	26.3 - 3.901
3	.609	-.0644	23.10	-5.99	-6.93	1.64	16.17	-4.35	27.0 - 4.291
4	.314	-.0333	11.80	-3.08	-3.46	.84	8.34	-2.24	27.0 - 4.261
5	0	0	0	0	0	0	0	0	

(d) Fourth cycle.

Station	1	2	3	4	5	6	7	8	9	10
	$\phi^{(4)}_{a2R}$	$\phi^{(4)}_{a2I}$	$\phi^{(4)}_{bR}$	$\phi^{(4)}_{bI}$	$\phi^{(4)}_{blR}$	$\phi^{(4)}_{blI}$	$\phi^{(5)}_{a2R}$	$\phi^{(5)}_{a2I}$	$\frac{\phi^{(5)}_{a2R} + i\phi^{(5)}_{a2I}}{\phi^{(4)}_{a2R} + i\phi^{(4)}_{a2I}}$	$\frac{\sum\left(\phi^{(5)}_{a2R} + i\phi^{(5)}_{a2I}\right)}{\sum\left(\phi^{(4)}_{a2R} + i\phi^{(4)}_{a2I}\right)}$
			$\frac{\lambda_o^4 \gamma}{EI\mu}\frac{1}{C}$							
1	1.000	0	33.16	-8.75	-6.03	4.68	27.13	-4.07	27.13 - 4.071	
2	.901	-.0256	30.70	-8.15	-6.33	3.80	24.37	-4.35	27.1 - 4.051	
3	.624	-.0749	23.92	-6.30	-6.98	1.73	16.94	-4.57	27.7 - 4.021	27.3 - 4.051
4	.322	-.0384	12.20	-3.24	-3.49	.88	8.71	-2.36	27.5 - 4.061	
5	0	0	0	0	0	0	0	0		

$$\frac{1}{2}\left[\frac{\sum\left(y^{(5)}_{a2R} + iy^{(5)}_{a2I}\right)}{\sum\left(y^{(4)}_{a2R} + iy^{(4)}_{a2I}\right)} + \frac{\sum\left(\phi^{(5)}_{a2R} + i\phi^{(5)}_{a2I}\right)}{\sum\left(\phi^{(4)}_{a2R} + i\phi^{(4)}_{a2I}\right)}\right] = (28.9 - 3.781)\frac{\lambda_o^4 \gamma}{EI\mu}\frac{1}{C};\ \omega_2 = 121.0 \text{ radians per second};\ g_{a2} = -0.1308;\ v_2 = 280 \text{ feet per second}$$

TABLE 7.- ITERATION TO OBTAIN TRANSFORMED THIRD MODE FOR $k = 0.1443$. WING WITH CONCENTRATED MASS.

[Common factors for each column are given under the column headings.]

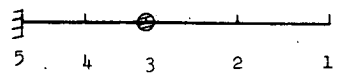

Flexure: (a) First cycle.

Station	1	2	3	4	5	6	7	8	9	10	11
	$y^{(1)}_{a3R}$	$y^{(1)}_{a3I}$	$y^{(1)}_{bR}$	$y^{(1)}_{bI}$	$y^{(1)}_{b1R}$	$y^{(1)}_{b1I}$	$y^{(1)}_{ba2R}$	$y^{(1)}_{ba2I}$	$y^{(2)}_{a3R}$	$y^{(2)}_{a3I}$	$\frac{y^{(2)}_{a3R} + iy^{(2)}_{a3I}}{y^{(1)}_{a3R} + iy^{(1)}_{a3I}}$
	b		$\frac{\lambda_o^4 b\gamma}{EI\mu}\frac{1}{C}$								$\frac{\lambda_o^4\gamma}{EI\mu}\frac{1}{C}$
1(A)	0	0	368.1	-73.82	-368.1	73.82	0	0	0	0	
2	.850	0	223.1	-43.43	-209.2	41.05	-2.7	1.37	11.2	-1.01	------
3	1.000	0	85.4	-15.60	-71.5	13.26	-2.3	1.45	11.6	-.89	11.6 - 0.89i
4	.350	0	25.4	-4.45	-20.1	3.59	-.9	.57	4.4	-.29	------
5	0	0	0	0	0	0	0	0	0	0	

(b) Second cycle.

1	2	3	4	5	6	7	8	9	10	11
$y^{(2)}_{a3R}$	$y^{(2)}_{a3I}$	$y^{(2)}_{bR}$	$y^{(2)}_{bI}$	$y^{(2)}_{b1R}$	$y^{(2)}_{b1I}$	$y^{(2)}_{ba2R}$	$y^{(2)}_{ba2I}$	$y^{(3)}_{a3R}$	$y^{(3)}_{a3I}$	$\frac{y^{(3)}_{a3R} + iy^{(3)}_{a3I}}{y^{(2)}_{a3R} + iy^{(2)}_{a3I}}$
b		$\frac{\lambda_o^4 b\gamma}{EI\mu}\frac{1}{C}$								$\frac{\lambda_o^4\gamma}{EI\mu}\frac{1}{C}$
0	0	484.0	-83.49	-484.0	83.49	0	0	0	0	
.967	-.013	296.2	-48.57	-274.8	46.14	-4.5	2.08	16.9	-.35	17.5 - 0.13i
1.000	0	113.0	-16.82	-93.9	14.80	-3.8	2.23	15.3	.21	15.3 + 0.21i
.379	.004	34.4	-4.73	-26.3	3.97	-1.4	.88	6.6	.12	------
0	0	0	0	0	0	0	0	0	0	

Torsion: (a) First cycle.

Station	1	2	3	4	5	6	7	8	9	10	11
	$\phi^{(1)}_{a3R}$	$\phi^{(1)}_{a3I}$	$\phi^{(1)}_{bR}$	$\phi^{(1)}_{bI}$	$\phi^{(1)}_{b1R}$	$\phi^{(1)}_{b1I}$	$\phi^{(1)}_{ba2R}$	$\phi^{(1)}_{ba2I}$	$\phi^{(2)}_{a3R}$	$\phi^{(2)}_{a3I}$	$\frac{\phi^{(2)}_{a3R} + i\phi^{(2)}_{a3I}}{\phi^{(1)}_{a3R} + i\phi^{(1)}_{a3I}}$
			$\frac{\lambda_o^4\gamma}{EI\mu}\frac{1}{C}$								
1(B)	0	0	-10.24	1.687	2.32	-1.897	7.92	0.210	0	0	
2	0	0	-10.30	1.592	2.45	-1.551	7.15	-.010	-.70	.031	------
3	0	0	-10.60	1.067	2.72	-.742	5.05	-.445	-2.83	-.120	------
4	0	0	-5.28	.564	1.36	-.378	2.60	-.231	-1.32	-.045	------
5	0	0	0	0	0	0	0	0	0	0	

(b) Second cycle.

1	2	3	4	5	6	7	8	9	10	11
$\phi^{(2)}_{a3R}$	$\phi^{(2)}_{a3I}$	$\phi^{(2)}_{bR}$	$\phi^{(2)}_{bI}$	$\phi^{(2)}_{b1R}$	$\phi^{(2)}_{b1I}$	$\phi^{(2)}_{ba2R}$	$\phi^{(2)}_{ba2I}$	$\phi^{(3)}_{a3R}$	$\phi^{(3)}_{a3I}$	$\frac{\phi^{(3)}_{a3R} + i\phi^{(3)}_{a3I}}{\phi^{(2)}_{a3R} + i\phi^{(2)}_{a3I}}$
		$\frac{\lambda_o^4\gamma}{EI\mu}\frac{1}{C}$								
0	0	-15.99	1.640	3.12	-2.392	12.87	0.752	0	0	
-.060	-.0019	-16.02	1.521	3.26	-1.938	11.61	.358	-1.15	-.059	------
-.241	-.0289	-16.00	.858	3.59	-.872	8.23	-.460	-4.18	-.474	17.4 - 0.116i
-.113	-.0125	-8.07	.472	1.80	-.445	4.23	-.242	-2.04	-.215	18.0 - 0.093i
0	0	0	0	0	0	0	0	0	0	

TABLE 7.- ITERATION TO OBTAIN TRANSFORMED THIRD MODE FOR $k = 0.1443$. WING WITH CONCENTRATED MASS - Concluded

Flexure: (c) Third cycle.

Station	1	2	3	4	5	6	7	8	9	10	11
	$y^{(3)}_{a3R}$	$y^{(3)}_{a3I}$	$y^{(3)}_{bR}$	$y^{(3)}_{bI}$	$y^{(3)}_{blR}$	$y^{(3)}_{blI}$	$y^{(3)}_{ba2R}$	$y^{(3)}_{ba2I}$	$y^{(4)}_{a3R}$	$y^{(4)}_{a3I}$	$\frac{y^{(4)}_{a3R}+iy^{(4)}_{a3I}}{y^{(3)}_{a3R}+iy^{(3)}_{a3I}}$
	b		$\frac{\lambda_o^4 b\gamma}{EI\mu}\frac{1}{C}$								$\frac{\lambda_o^4\gamma}{EI\mu}\frac{1}{C}$
1(A)	0	0	515.9	-102.86	-515.9	102.86	0	0	0	0	
2	1.105	-.038	311.8	-59.83	-293.8	57.3	-4.6	2.21	13.4	-.29	12.2 + 0.161
3	1.000	0	118.5	-20.69	-100.5	18.51	-3.9	2.37	14.1	.19	14.1 + 0.191
4	.431	.002	35.2	-5.93	-28.2	5.00	-1.5	.93	5.5	0	12.7 - 0.061
5	0	0	0	0	0	0	0	0	0	0	

(d) Fourth cycle.

Station	1	2	3	4	5	6	7	8	9	10	11	12
	$y^{(4)}_{a3R}$	$y^{(4)}_{a3I}$	$y^{(4)}_{bR}$	$y^{(4)}_{bI}$	$y^{(4)}_{blR}$	$y^{(4)}_{blI}$	$y^{(4)}_{ba2R}$	$y^{(4)}_{ba2I}$	$y^{(5)}_{a3R}$	$y^{(5)}_{a3I}$	$\frac{y^{(5)}_{a3R}+iy^{(5)}_{a3I}}{y^{(4)}_{a3R}+iy^{(4)}_{a3I}}$	$\frac{\sum\left(y^{(5)}_{a3R}+iy^{(5)}_{a3I}\right)}{\sum\left(y^{(4)}_{a3R}+iy^{(4)}_{a3I}\right)}$
	b		$\frac{\lambda_o^4 b\gamma}{EI\mu}\frac{1}{C}$								$\frac{\lambda_o^4\gamma}{EI\mu}\frac{1}{C}$	
1(A)	0	0	494.8	-86.24	-494.8	86.24	0	0	0	0		
2	.952	-.033	300.3	-50.13	-281.6	47.75	-5.1	2.35	13.6	-.03	14.3 +0.461	
3	1.000	0	115.2	-17.33	-96.2	15.31	-4.3	2.53	14.7	.51	14.7 + 0.511	14.53 + 0.547i
4	.390	-.005	34.4	-4.87	-26.9	4.12	-1.7	1.00	5.8	.25	14.8 + 0.83i	
5	0	0	0	0	0	0	0	0	0	0		

Torsion: (c) Third cycle.

Station	1	2	3	4	5	6	7	8	9	10	11
	$\phi^{(3)}_{a3R}$	$\phi^{(3)}_{a3I}$	$\phi^{(3)}_{bR}$	$\phi^{(3)}_{bI}$	$\phi^{(3)}_{blR}$	$\phi^{(3)}_{blI}$	$\phi^{(3)}_{ba2R}$	$\phi^{(3)}_{ba2I}$	$\phi^{(4)}_{a3R}$	$\phi^{(4)}_{a3I}$	$\frac{\phi^{(4)}_{a3R}+i\phi^{(4)}_{a3I}}{\phi^{(3)}_{a3R}+i\phi^{(3)}_{a3I}}$
			$\frac{\lambda_o^4\gamma}{EI\mu}\frac{1}{C}$								
1(B)	0	0	-16.73	1.942	3.26	-2.658	13.47	0.716	0	0	
2	-.075	-.0028	-16.78	1.808	3.44	-2.174	12.17	.300	-1.17	-.066	15.6 + 0.301
3	-.273	-.0272	-16.72	1.053	3.82	-1.037	8.63	-.533	-4.27	-.517	15.7 + 0.331
4	-.134	-.0122	-8.45	.577	1.91	-.529	4.43	-.279	-2.11	-.231	15.8 + 0.291
5	0	0	0	0	0	0	0	0	0	0	

(d) Fourth cycle.

Station	1	2	3	4	5	6	7	8	9	10	11	12
	$\phi^{(4)}_{a3R}$	$\phi^{(4)}_{a3I}$	$\phi^{(4)}_{bR}$	$\phi^{(4)}_{bI}$	$\phi^{(4)}_{blR}$	$\phi^{(4)}_{blI}$	$\phi^{(4)}_{ba2R}$	$\phi^{(4)}_{ba2I}$	$\phi^{(5)}_{a3R}$	$\phi^{(5)}_{a3I}$	$\frac{\phi^{(5)}_{a3R}+i\phi^{(5)}_{a3I}}{\phi^{(4)}_{a3R}+i\phi^{(4)}_{a3I}}$	$\frac{\sum\left(\phi^{(5)}_{a3R}+i\phi^{(5)}_{a3I}\right)}{\sum\left(\phi^{(4)}_{a3R}+i\phi^{(4)}_{a3I}\right)}$
			$\frac{\lambda_o^4\gamma}{EI\mu}\frac{1}{C}$									
1(B)	0	0	-17.68	1.629	3.18	-2.460	14.50	0.831	0	0		
2	-.083	-.0036	-17.70	1.511	3.33	-1.992	13.09	.385	-1.28	-.096	15.4 + 0.49i	
3	-.304	-.0326	-17.53	.843	3.67	-.901	9.28	-.530	-4.58	-.588	15.1 + 0.321	15.12+ 0.343i
4	-.150	-.0144	-8.86	.470	1.84	-.459	4.77	-.278	-2.25	-.267	15.1 + 0.33i	
5	0	0	0	0	0	0	0	0	0	0		

$$\frac{1}{2}\left[\frac{\sum\left(y^{(5)}_{a3R}+iy^{(5)}_{a3I}\right)}{\sum\left(y^{(4)}_{a3R}+iy^{(4)}_{a3I}\right)}+\frac{\sum\left(\phi^{(5)}_{a3R}+i\phi^{(5)}_{a3I}\right)}{\sum\left(\phi^{(4)}_{a3R}+i\phi^{(4)}_{a3I}\right)}\right] = (14.82 + 0.445i)\frac{\lambda_o^4\gamma}{EI\mu}\frac{1}{C};\ \omega_3 = 168.9 \text{ radians per second};\ g_{a3} = 0.030;\ v_3 = 390 \text{ feet per second}$$

NACA

TABLE 8.- COMPUTATION OF TRUE SECOND MODE FOR $k = 0.1443$.

WING WITH CONCENTRATED MASS.

[Flexural functions are in terms of b; torsional functions are in radians. $\frac{C_1}{C_2} - 1 = F_{12} = 8.65 - 1.600i$.]

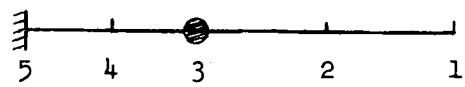

Flexure

Station	1	2	3	4
	$y^{(4)}_{b1R} + iy^{(4)}_{b1I} = F_{12}(y_{1R} + y_{1I})$	$y_{1R} + iy_{1I}$	$y^{(5)}_{a2R} + iy^{(5)}_{a2I}$	$y_{2R} + iy_{2I}$
1(A)	941.0 - 165.58i	108.8 + 0.96i	0	108.8 + 0.96i
2	----------	61.7 + 0.85i	-8.4 + 6.3i	53.3 + 7.15i
3	----------	21.06 + 0.49i	-6.9 + 6.32i	14.2 + 6.81i
4	----------	5.90 + 0.18i	-2.7 + 2.49i	3.2 + 2.67i
5	----------	0	0	0

Torsion

Station	1	2	3	4
	$\phi^{(4)}_{b1R} + i\phi^{(4)}_{b1I} = F_{12}(\phi_{1R} + i\phi_{1I})$	$\phi_{1R} + i\phi_{1I}$	$\phi^{(5)}_{a2R} + i\phi^{(5)}_{a2I}$	$\phi_{2R} + i\phi_{2I}$
1(B)	----------	-0.772 + 0.401i	27.13 - 4.07i	26.36 - 3.67i
2	----------	-0.786 + 0.294i	24.37 - 4.35i	23.58 - 4.06i
3	----------	-0.816 + 0.048i	16.94 - 4.57i	16.12 - 4.52i
4	----------	-0.409 + 0.026i	8.71 - 2.36i	8.30 - 2.33i
5	----------	0	0	0

TABLE 9.- COMPUTATION OF TRUE THIRD MODE FOR $k = 0.1443$. WING WITH CONCENTRATED MASS.

[Flexural functions are in terms of b; torsional functions are in radians. $\frac{C_1}{C_3} - 1 = F_{13} = 16.97 - 6.091i$; $\frac{C_2}{C_3} - 1 = F_{23} = 0.940 - 0.3131i$.]

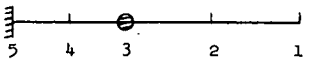

Station

Flexure

Station	1	2	3	4	5	6	7	8	9	10
	$y^{(4)}_{b1R} + iy^{(4)}_{b1I} = F_{13}(y_{11R} + iy_{11I}) + F_{23}(y_{12R} + iy_{12I})$	$y^{(4)}_{ba2R} + iy^{(4)}_{ba2I} = F_{23}(y_{a2R} + iy_{a2I})$	$F_{23}(y_{12R} + iy_{12I})$	$F_{13}(y_{11R} + iy_{11I})$	$y_{12R} + iy_{12I}$	$y_{11R} + iy_{11I}$	$y_{1R} + iy_{1I}$	$y_{a2R} + iy_{a2I}$	$y^{(5)}_{a3R} + iy^{(5)}_{a3I}$	$y_{3R} + iy_{3I}$
1(A)	-494.8 + 86.24i	--------	56.3 + 12.30i	-551.1 + 73.94i	50.1 + 29.71	-30.2 - 6.51i	19.9 + 23.21i	0	0	19.9 + 23.21i
2	---------	--------	---------	---------	--------	--------	11.26 + 13.23i	-5.56 + 0.64i	13.6 - 0.03i	19.3 + 13.84i
3	---------	--------	---------	---------	--------	--------	3.80 + 4.56i	-4.87 + 1.05i	14.7 + 0.51i	13.6 + 6.12i
4	---------	--------	---------	---------	--------	--------	1.06 + 1.28i	-1.91 + 0.42i	5.8 + 0.25i	5.0 + 1.95i
5	---------	--------	---------	---------	--------	--------	0	0	0	0

Torsion

Station	1	2	3	4	5	6	7	8	9	10
	$\phi^{(4)}_{b1R} + i\phi^{(4)}_{b1I} = F_{13}(\phi_{11R} + i\phi_{11I}) + F_{23}(\phi_{12R} + i\phi_{12I})$	$\phi^{(4)}_{ba2R} + i\phi^{(4)}_{ba2I} = F_{23}(\phi_{a2R} + i\phi_{a2I})$	$F_{23}(\phi_{12R} + i\phi_{12I})$	$F_{13}(\phi_{11R} + i\phi_{11I})$	$\phi_{12R} + i\phi_{12I}$	$\phi_{11R} + i\phi_{11I}$	$\phi_{1R} + i\phi_{1I}$	$\phi_{a2R} + i\phi_{a2I}$	$\phi^{(5)}_{a3R} + i\phi^{(5)}_{a3I}$	$\phi_{3R} + i\phi_{3I}$
1(B)	----------	14.50 + 0.83i	---------	---------	--------	--------	-0.227 - 0.089i	13.58 + 5.43i	0	13.35 + 5.34i
2	---------	--------	---------	---------	--------	--------	-0.208 - 0.113i	12.37 + 4.55i	-1.28 - 0.096i	10.88 + 4.34i
3	---------	--------	---------	---------	--------	--------	-0.162 - 0.164i	9.03 + 2.46i	-4.58 - 0.588i	4.29 + 1.71i
4	---------	--------	---------	---------	--------	--------	-0.081 - 0.081i	4.64 + 1.25i	-2.25 - 0.267i	2.31 + 0.90i
5	---------	--------	---------	---------	--------	--------	0	0	0	0

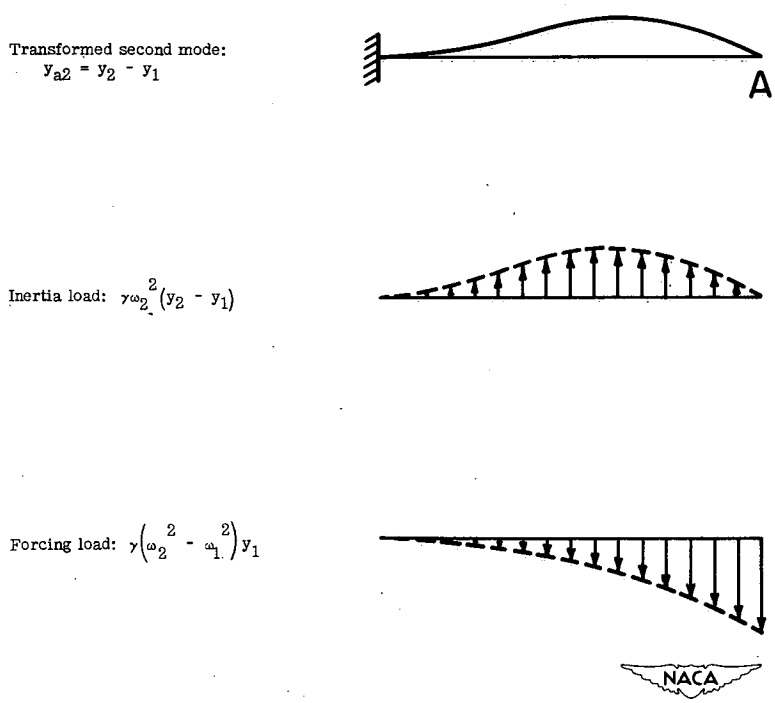

Figure 1.- Illustration of physical basis of iterative transformation procedure.

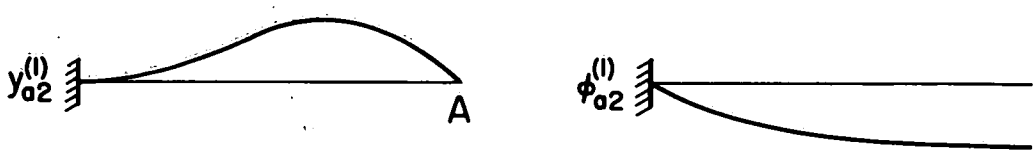

(a) Assumed transformed second mode.

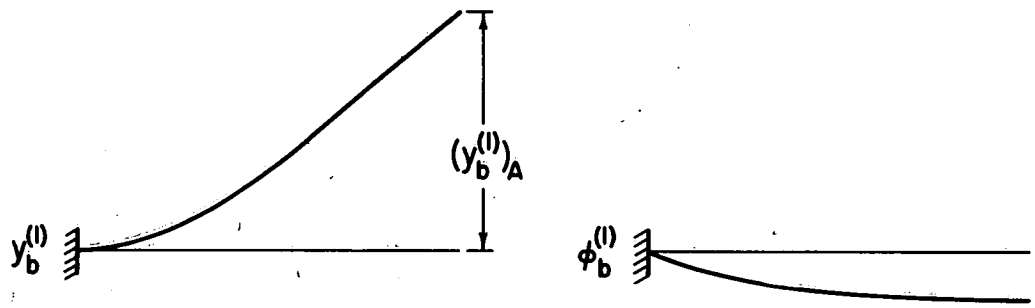

(b) Intermediate derived mode.

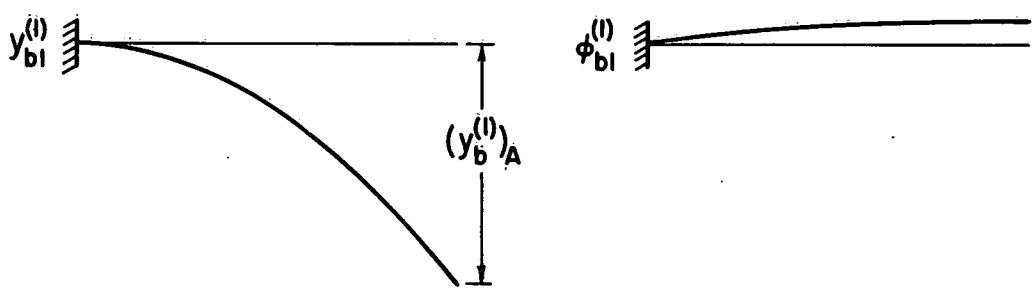

(c) First-mode sweeping function.

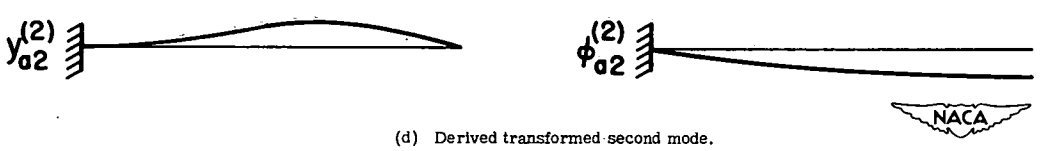

(d) Derived transformed second mode.

Figure 2.- Illustration of steps in the iterative transformation procedure for determining coupled modes.

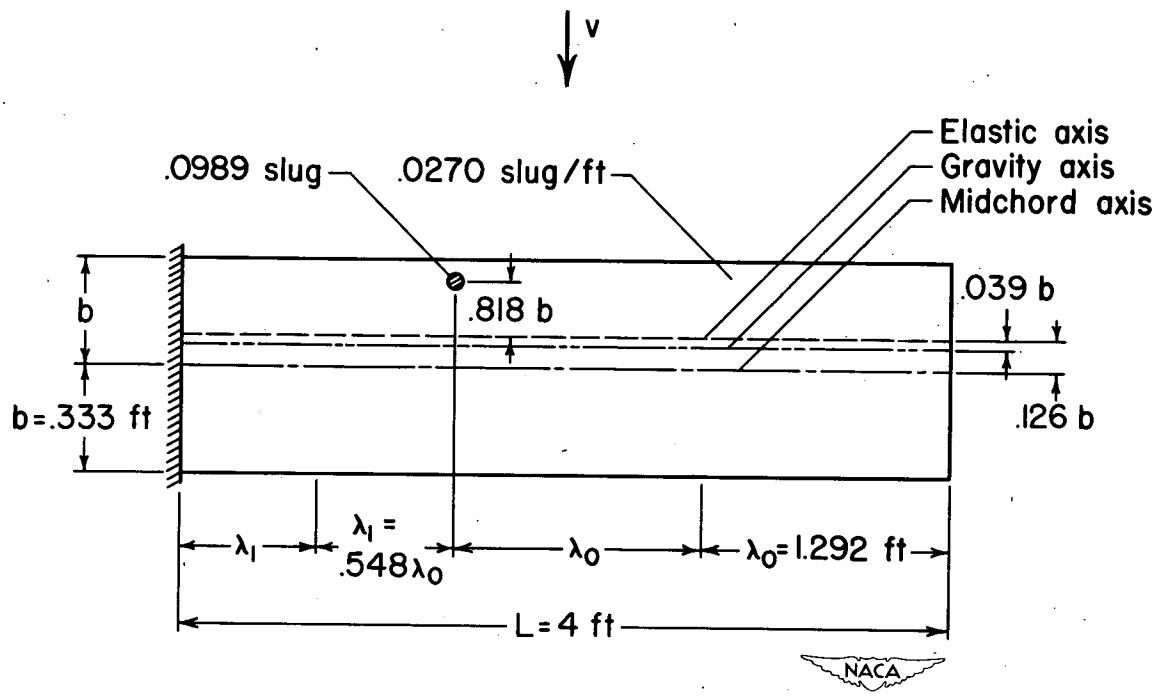

$\rho = 0.002378$ slug/ft^3

$\mu = 32.6$

$EI = 977.1$ lb-ft^2

$GJ = 480.6$ lb-ft^2

$$\frac{EI\mu}{\lambda_o^4 \gamma} = 423{,}000 \text{ (radians/sec)}^2$$

$$\left(\frac{b}{\lambda_o}\right)^2 \frac{EI}{GJ} = 0.1353$$

Figure 3.- Properties of cantilever wing used in numerical examples.

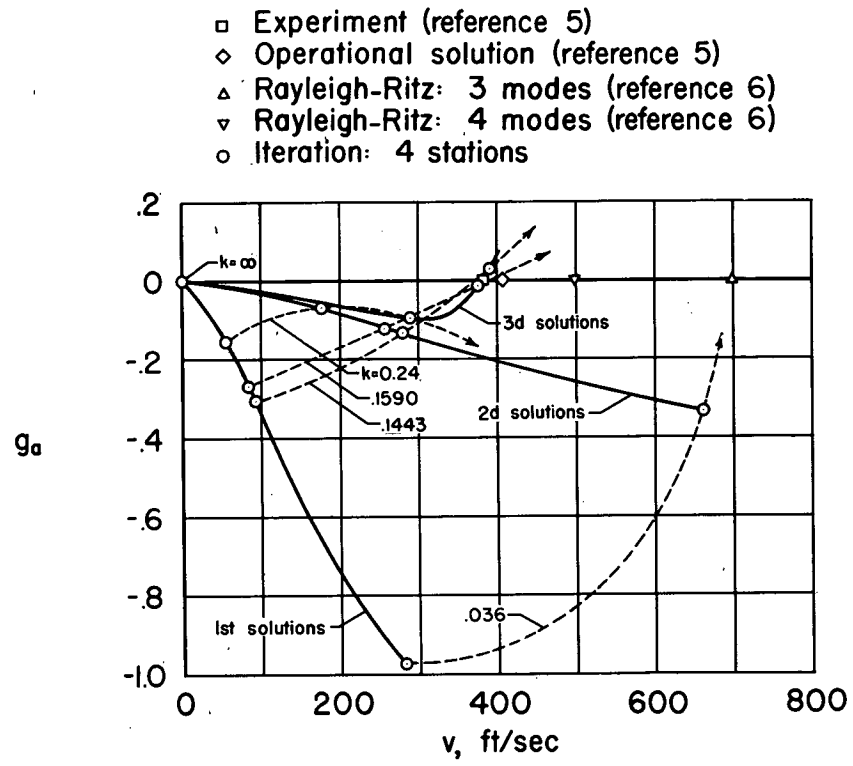

(a) Variation of artificial damping with airspeed.

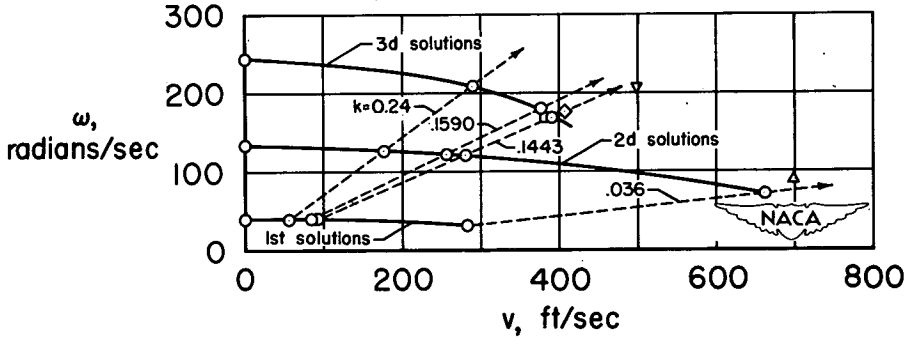

(b) Variation of frequency with airspeed.

Figure 4.- Variation of artificial damping and frequency with airspeed in first three solutions. Wing with concentrated mass.

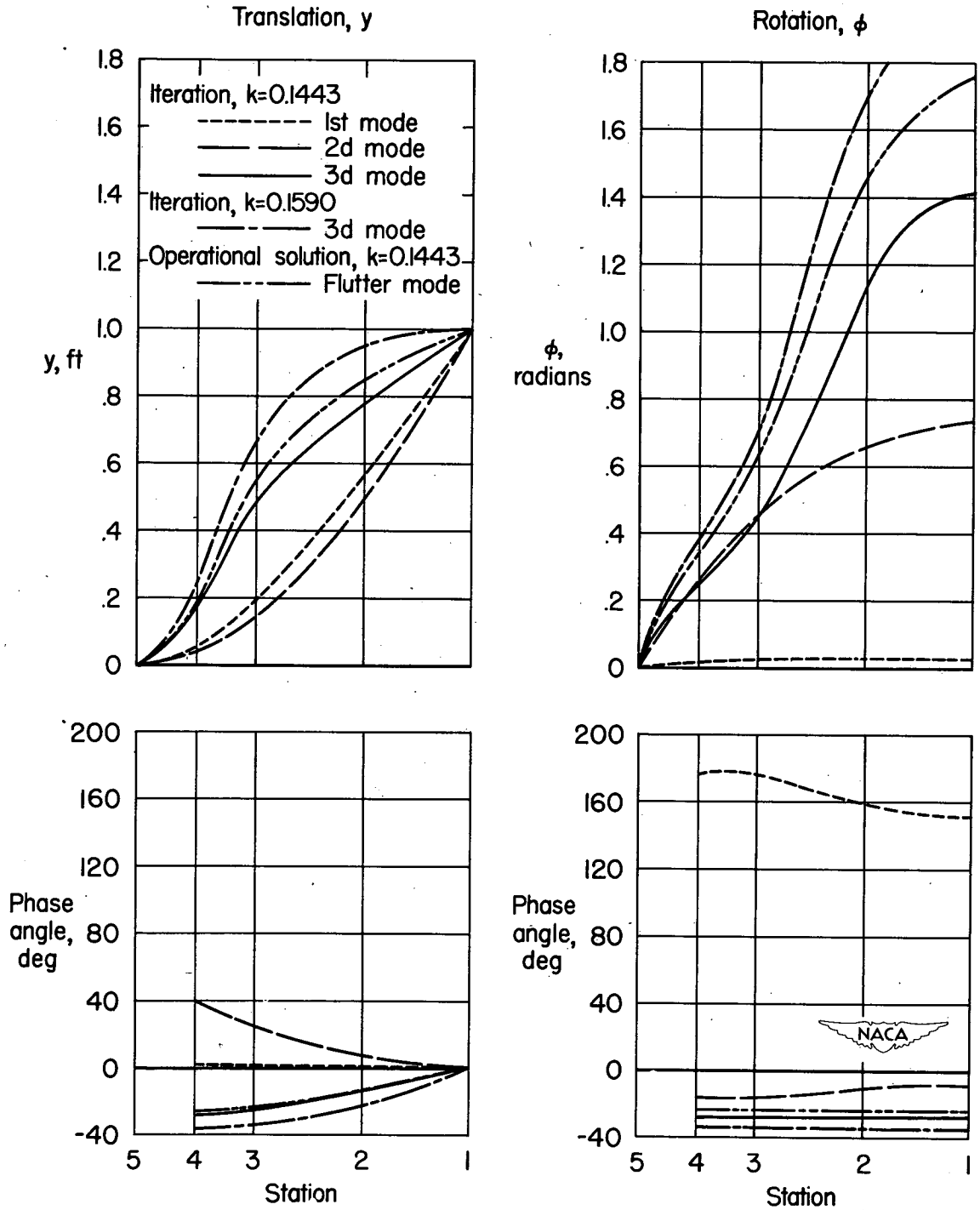

Figure 5.- Amplitudes and phases of modes. Wing with concentrated mass.

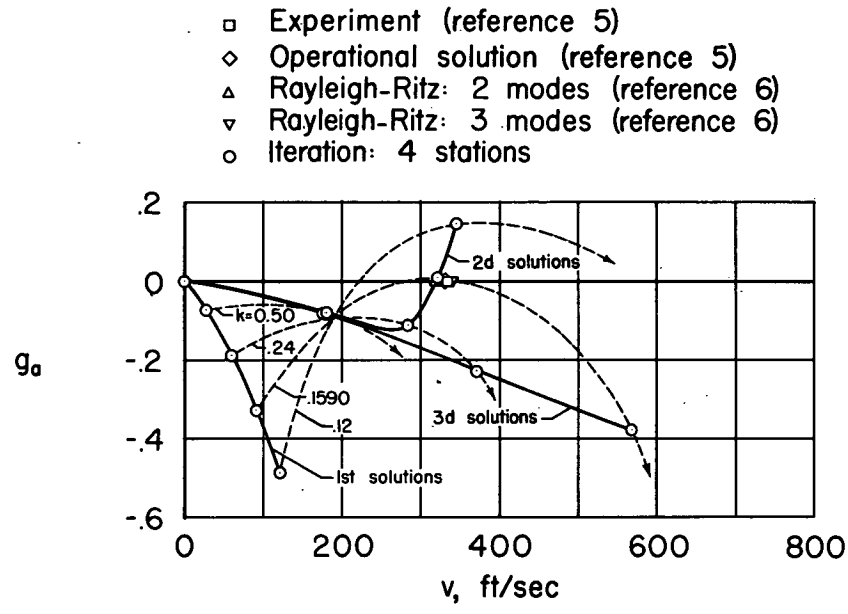

(a) Variation of artificial damping with airspeed.

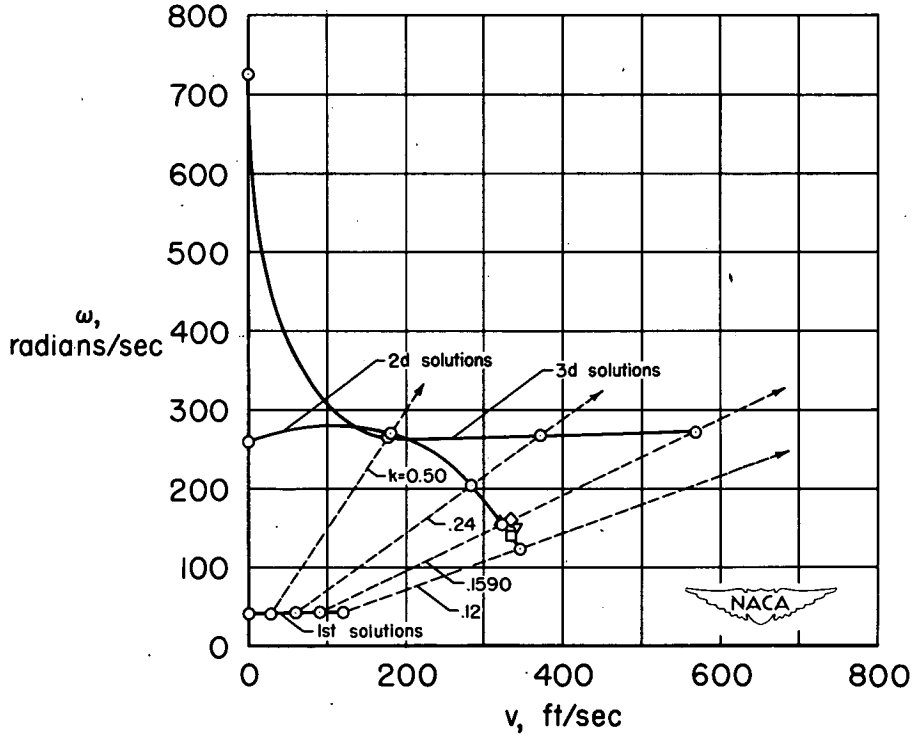

(b) Variation of frequency with airspeed.

Figure 6.- Variation of artificial damping and frequency in first three solutions. Wing without concentrated mass.

NACA-Langley - 5-16-51 -1000